RF PASSIVE CIRCUIT DESIGN WITH FLUIDIC TUNING

A THESIS
SUBMITTED TO THE FACULTY OF THE GRADUATE SCHOOL
OF THE UNIVERSITY OF MINNESOTA
BY

Glenston Hadlee Miranda

IN PARTIAL FULFILLMENT OF THE REQUIREMENTS
FOR THE DEGREE OF
MASTER OF SCIENCE

Advisor: Rhonda R. Franklin

September 2014

Acknowledgements

I would like to thank Dr. Rhonda Franklin for her valuable technical advice and guidance. Dr. Franklin has been an excellent mentor and her insights on research, industry and science has helped me overcome difficulties and struggles over the past 2 years. Dr Franklin's keen interest in her students' well-being has made the journey even more enjoyable.

I would like to thank Dr Robert Sainati for helping me with the Anechoic chamber radiation pattern measurements at 3M. I would also like to thank graduate committee members Dr. David Wood and Dr. Anand Gopinath for their time and effort serving on the committee. I would like to express my gratitude to MPACT group member Jordan Alstad, Casey Murray and Chanjoon Lee, for fielding my questions and concerns with patience and enthusiasm.

I am very appreciative of the support provided by Mark Fisher and Kevin Roberts of the Minnesota Nanofabrication Center at the University of Minnesota in my fabrication and fabrication challenges.

Many friends, including Mandip Sibakoti, have helped me through the sometimes stressful moments of graduate school, which has proven instrumental to my success. I would also like to thank my sister Hazel, for her endless support and friendship. I am forever indebted to my parents, Henry and Gracy Miranda, my grandmom Assumpta Miranda and my Godfather, Rajesh Kheny for always supporting me and shaping me into the person I am today.

This thesis is dedicated to
Assumpta, Henry, Gracy, Hazel Miranda and Rajesh Kheny

Abstract

This thesis discusses RF dielectric spectroscopy of fluids using microstrip line and coplanar waveguide as well as the use of RF fluids in passive RF circuits. The use of liquids as a tuning element and as a coolant is not very well explored. In this work different liquids are analyzed for its dielectric properties and its tuning capability. Several passive tuning circuits have been designed and developed, for example a tunable bandstop filter that uses liquids to shift the λ/4 resonance modes of the stub. In addition a patch antenna with the tunable liquid stub that uses the open end effect of the stub as a switch is fabricated and studied.

Table of Contents

List of Tables

List of Figures

CHAPTER 1

INTRODUCTION

1.1 Motivation

With the increased demand for high data rates and compact remote sensing, the RF power requirements increase substantially. This increase leads to high power dissipation as heat, causing major damage to devices and thereby putting the entire system at risk. Mechanisms and ways, to ensure that the active RF device/circuit in the system is kept below their threshold temperature is the need of the hour. To remove the heat generated by an embedded high power RF device or circuit, the following mechanisms and techniques have been used and still under investigation: a) inclusion of thermal vias that carry the heat away from the device to a heat sink [1]; b) inclusion of heat pipes through the substrate stack [2]; and c) inclusion of microchannels circulating a cooling fluid via a micropump [3]. Work on using a mixture of ethylene glycol and DI H_2O as a coolant on LCP substrates has been demonstrated in [4].

The technique with microchannels is gaining importance as the liquids used as a coolant can have the added advantage of providing tuning on printed circuit boards. Tuning provided by liquids have been used in reconfigurable design structures to tune antennas, filters and phase shifters [5-9]. In [5], fluid channels are placed along an annular slot antenna to change the circumference of the antenna. A band stop, 4 arm Archimedean spiral FSS is tuned using liquids [6]. A linear phase shifter using fluids is demonstrated in [7]. The variation in the columnar height of a colloidal suspension above an aluminum ground

plane is used in a reconfigurable dielectric coaxial resonator [8]. Liquids are used as tunable elements in the coupling gap of a directional coupler [9].

In all of the above work the liquid has been directly utilized on the operational structure (antenna, FSS and phase shifter) with the loss of the structure dependent on the dielectric loss of the liquid. The work presented here uses the liquids on a stub that is not connected to the direct signal, thereby ensuring that the dielectric loss of the liquid does not affect the overall propagation loss of the system. Further, different coolants that can be used for tuning and cooling have been investigated for their dielectric loss and tuning capability. Change of the above properties with heat is also investigated.

1.2 Design Overview

There are five main chapters in this thesis. The literature analysis of different liquids and development of the high frequency microstrip line test structures is discussed in Chapter 2. Chapter 3 investigates the variation in liquid properties with heat using coplanar waveguide test structures. Using one of the liquids (DI H_2O) from the study in Chapter 2 and Chapter 3, resonant circuit tuning capability is described in Chapter 4. Chapter 5 presents the use of a liquid as a tuning stub element in a patch antenna configuration. Future directions of this work and a summary of this thesis are provided in Chapter 6. The specific fabrication, testing, and theoretical work used herein are in the appendices.

CHAPTER 2

BACKGROUND OF FLUIDS AND DESIGN OF HIGH FREQUENCY MICROSTRIP LINE TEST STRUCTURES

2.1 Introduction

This chapter is devoted to the study on the background of the fluids used for tuning and its selection based on two criteria: loss and dielectric constant. The ideal tuning liquid should have high dielectric constant and low loss. It also needs to show low viscosity, similar to water [8.94x 10^{-4} Pa.s], to allow for free flow of liquid. No such liquid is found to fulfill the criteria, hence a compromise is made. Based on the research, Deionized Water (DI H_2O) [10], Ethylene Glycol [11] is chosen for their high dielectric constant and FC40 [12] is chosen for low loss. The S parameter analysis and dielectric constant extraction is discussed using the high frequency microstrip line test structure. There have been many different techniques that have been in use and still in research for dielectric spectroscopy [13-17]. A coplanar waveguide [13], microstrip line [14-15], coaxial resonator [16] and capacitive divider [17] have been used for extracting complex dielectric permittivity of microliter to nanoliter liquid samples. In this chapter the emphasis is on bulk liquid testing and the technique used will be that of microstrip line for ease of fabrication and analysis.

2.1.1 Deionized Water (DI H_2O)

Deionized water has good ability to transfer heat and is thermally non-conductive. The tradeoff is that DI H_2O also suffers from the fact that it vaporizes at 100°C [10]. This means the pressure in the vessel containing the fluid will increase as the temperature approaches 100°C, causing the systems it flows through to experience expansion. Since it is likely the temperature of the RF device will have surface temperatures over 100°C

this issue must be considered and circulation may be needed to provide adequate cooling that does not destroy the electronic circuit system.

2.1.2 FC-40

FC-40 [12] is part of a family of fluids called Fluorinert for use in the semiconductor industry. These fluids are designed to be compatible with semiconductor materials and electronic circuits as a cooling medium. The viscosity of FC-40 is indiscernible in reference to water. The fluid, however, is not soluble with water and exhibits a strong polar response to water. FC-40 is significantly heavier than water at about 15 lbs. per US gallon in a liquid state from -57C to 155C. As a heat transfer medium, this fluid has high heat conductivity. The loss in this fluid is almost negligible; however, the relative permittivity is also low (~2).

2.1.3 Antifreeze

Antifreeze [18] is a common coolant used in automobiles and industrial facilities. The chemical makeup of antifreeze is usually about 97-99% ethylene glycol and 1-3% other chemicals. These other chemicals are added to provide for cleaning and corrosion prevention in the cooling loops utilizing this fluid. Antifreeze has high heat conductivity and is soluble in water, leading to the possibility of mixing these fluids together. The viscosity of antifreeze is only slightly lower than that of water. The main concern with antifreeze is the combination of chemicals in its makeup. Common additives include sodium silicate, disodium phosphate, sodium molybdate, sodium borate and dextrin (hydroxyethyl starch). These impurities vary between manufacturers and are not always compatible with electronic devices.

2.1.4 Ethylene Glycol

Ethylene Glycol [11] (EG) is the main ingredient in industrial and automotive antifreeze. In its pure form, EG is non-conductive and has a viscosity only slightly lower than that of water. EG is water soluble making it possible to mix this fluid with other fluids. Similar to antifreeze, ethylene glycol has high heat conductivity as compared to water. The loss of this fluid is found to be significant beyond 3GHz in testing.

2.1.5 Industrial Dielectric Fluid

Industrial Dielectric Fluid (IDF) is used in an industry specific cooling application. IDF is non-conductive as a dielectric fluid. The viscosity of the fluid is similar to that of water making it possible for use in RF devices. The fluid is environmentally stable and has a flash point above 350^0C which makes it an efficient coolant at high temperatures. Because of its chemical design, it is not possible to mix this fluid with other fluids. The dielectric constant of the liquid is very low making it unsuitable for use in tuning.

2.2 Microstrip High Frequency Testing Circuit for Fluid Characterization

The fluids in this study is characterized with a microstrip transmission line circuit technology due to ease of manufacturing and available knowledge on characterization of RF electronic circuit materials. They are measured using an Anritsu 37369D Network Analyzer. The frequency range is between 40MHz and 20GHz. The schematic of the microstrip line with the superstrate is seen in Fig. 2.1[19].

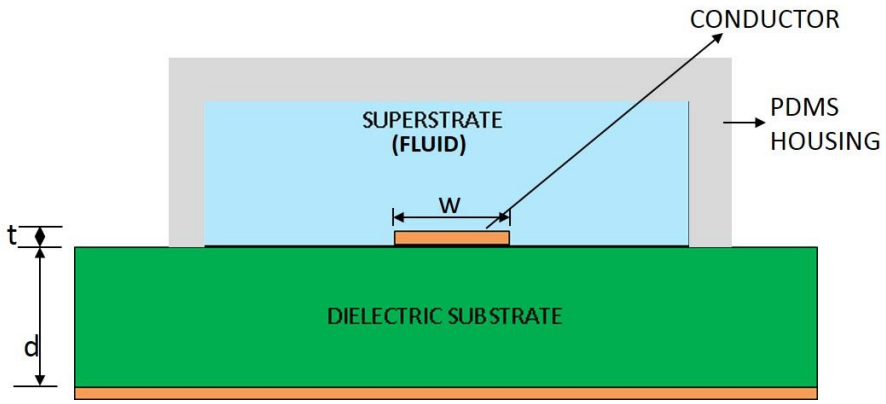

Figure 2.1. Cross section of microstrip line with the PDMS housing (in grey) and the superstrate (fluid in blue).

2.2.1 Design of the Microstrip RF Fluid Characterization Apparatus

The fluid is poured into a 4L Pirex Beaker. The complete setup with fluid in the beaker can be seen in Fig. 2.2. The physical circuit layout is designed to allow the line to be fully submerged in the fluid under test, and isolate the leads of the Network Analyzer from the fluid. To address this design requirement, the line is created on a U-Shape substrate with beveled corners as seen in Fig. 2.3.

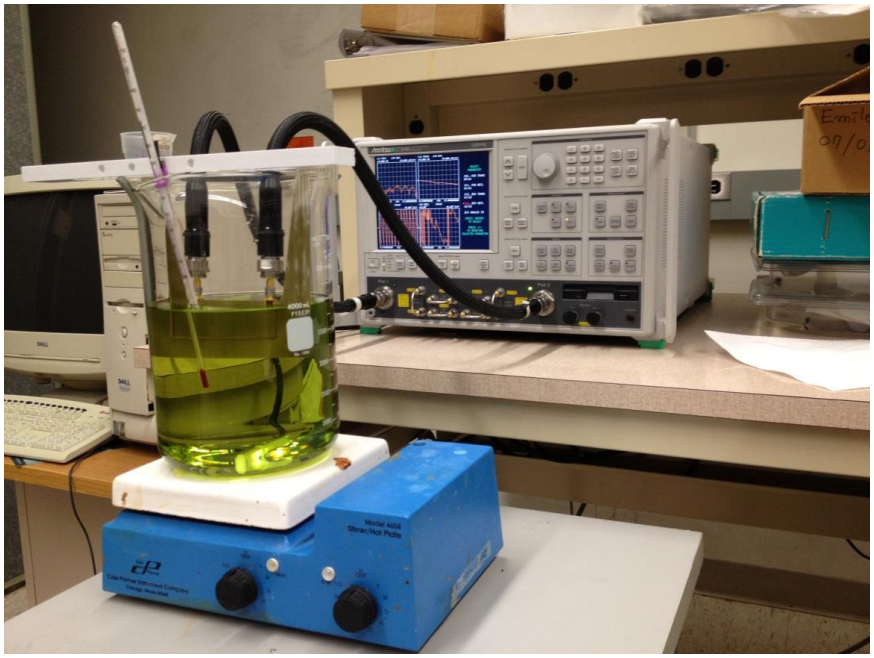

Figure 2.2. Microstrip high frequency test setup, with the microstrip line connected to the network analyzer and placed on a hot plate with a thermometer placed inside the beaker.

The test circuit is printed at the base of the U-shaped substrate also in a U-shaped configuration. The U-Shaped line, fabricated on a larger U-Shaped FR4 board substrate, allows the device to hang into the solution and for the SMA connectors to be placed on the edge of the FR4 board for the electrical measurement, while the substrate, which also acts as a holder, can hang from the top of a 4L PIREX Beaker. This design is documented in Fig. 2.3. All designs (TLine and substrate structure) use the layout tool in ADS [20] to create an exported file that is fed to a computer controlled LPKF PhotoMat C60 Milling Machine [21].

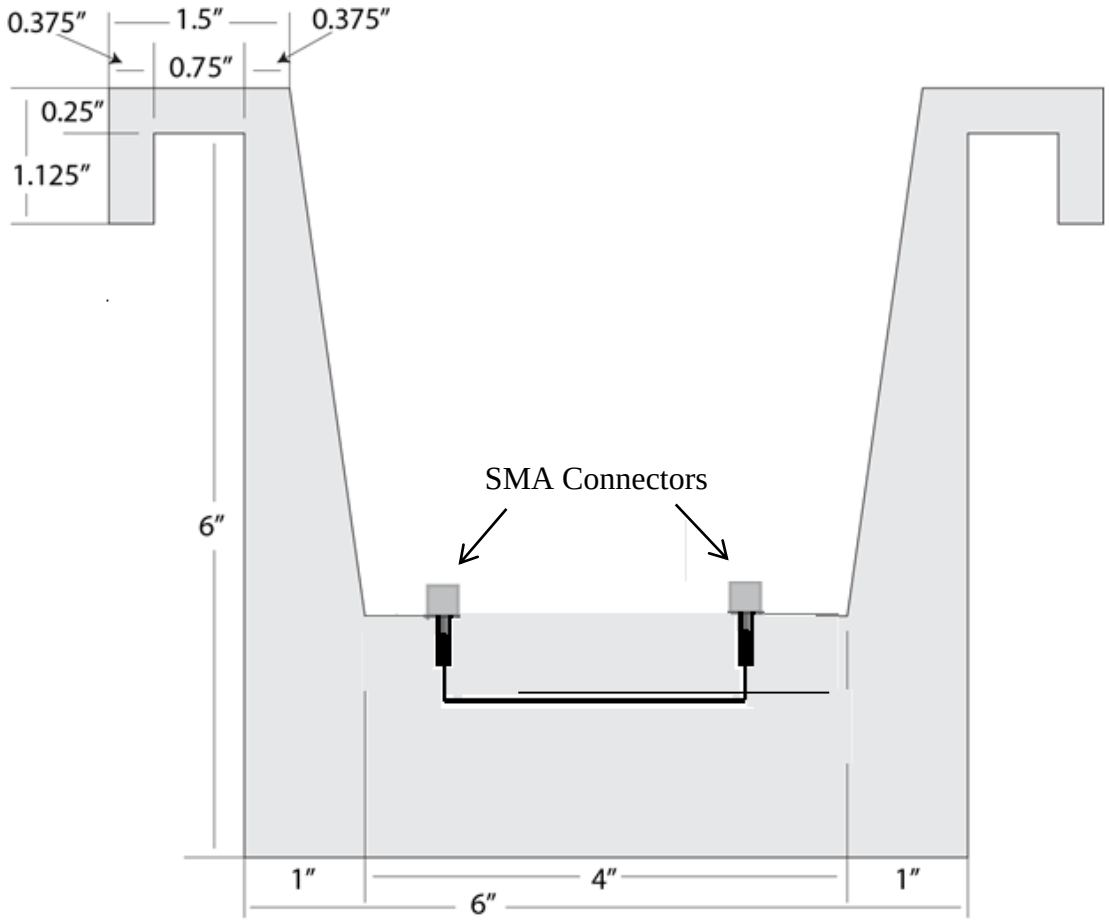

Figure 2.3. Microstrip line substrate design and dimensions. U-Hook on right is symmetrical with the left. The approximate placement of microstrip line relative to the substrate is shown here.

2.2.2 Design of Microstrip Test Circuits for Fluid Characterization

Two transmission line configurations are used to study the S parameters of the microstrip line when immersed in the liquid:-(a) no transition (U) (b) with transition (T) shown in Fig. 2.4 a and b. Each circuit contains a feedline, to which the SMA connector is soldered and the transmission (TX) line section, where evaluation of the fluid occurs. The feed line section width is represented as W1 in design U and W2 in design T. The transmission line section width is represented as W1 for both the U and the T designs. W1 width is chosen such that it produces 50 ohms in the liquid and W2 is designed to produce 50 ohms in air. For liquids with dielectric constant less than 5, the W2 width is close to W1. This ends up with the liquid having just one design, i.e. no transition (U). Fig. 2.5 shows the fabricated design board for FC40 (ε_r=1.9) [12], where W1 is 107.64 mils (50 ohms in FC40) and W2 is 108.75 mils (50 ohms in air). Since the resolution of the milling machine is 5 mils, the transition is not seen. For liquids with dielectric constant above 30, W1 is 27 mils and W2 is 107.25 mils. Therefore, we have 2 design configurations for such a liquid a) no transition (U), with W1 width for both feedline and transmission line section as seen in Fig. 2.6(a), b) transition (T) with W2 to feedline and W1 to transmission line as seen in Fig. 2.6(b). In Fig. 2.4(b), the transmission width (W1) produces an impedance of 50 ohms in the liquid, while transmission line width (W2) is designed to produce an impedance of 50 ohms in air. The design algorithm to generate the width of the line is demonstrated in Section 2.3. For the case of DI H_2O (ε_r=78, at 3 GHz) [10] as seen in Fig. 2.6(b), the narrow line (W1=27.025 mils) produces an impedance of 95 ohms in air and 50 ohms when submerged in DI H_2O. To summarize, W1 width is chosen such that it produces 50 ohms in the liquid and W2 is designed to produce 50 ohms in air.

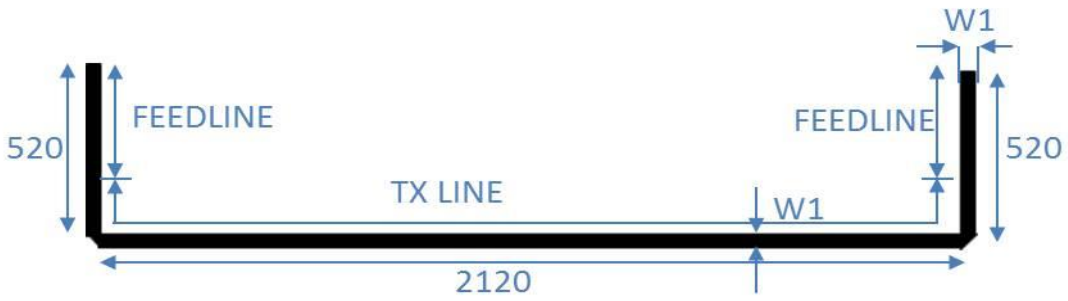

a) U(without transition)

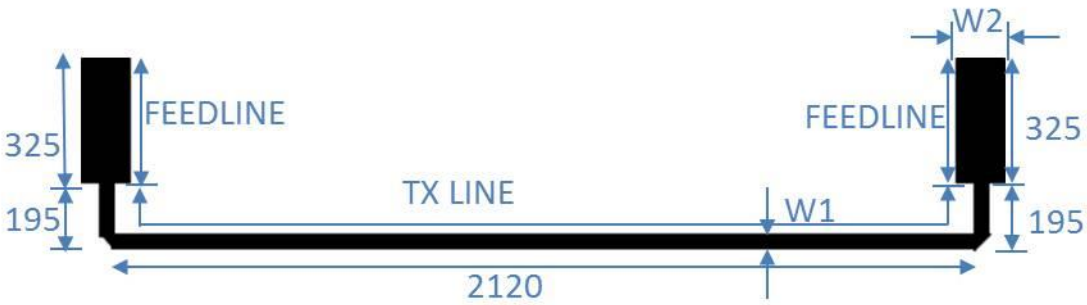

b) T(with transition)

Figure 2.4:- Two different designs for liquid medium above the substrate a) uniform, where W1 is used for feedline section and transmission line section b) transition, where W2 is used for feedline section and W1 is used for transmission line section. All the dimensions are in mils

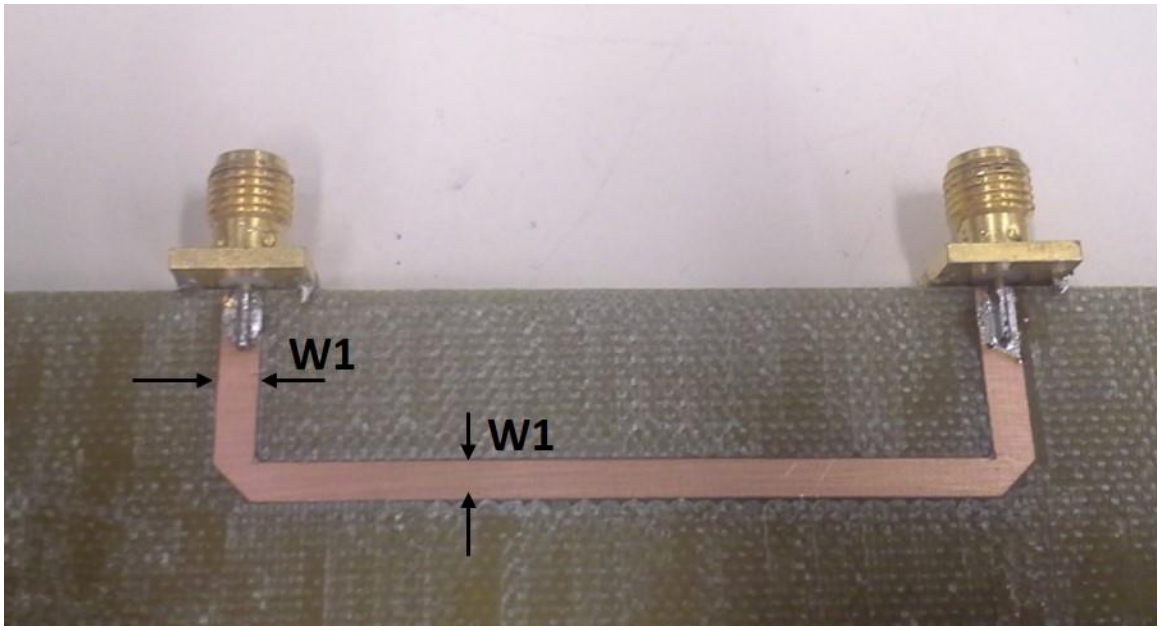

Figure 2.5. The circuit built for the design with FC40 as the surrounding medium. The width of the line is 108.75 mils. The difference between the dielectric constant of air and FC40, being very small, the board is uniform and forms a 50 ohm impedance both in air and when submerged in the fluid.

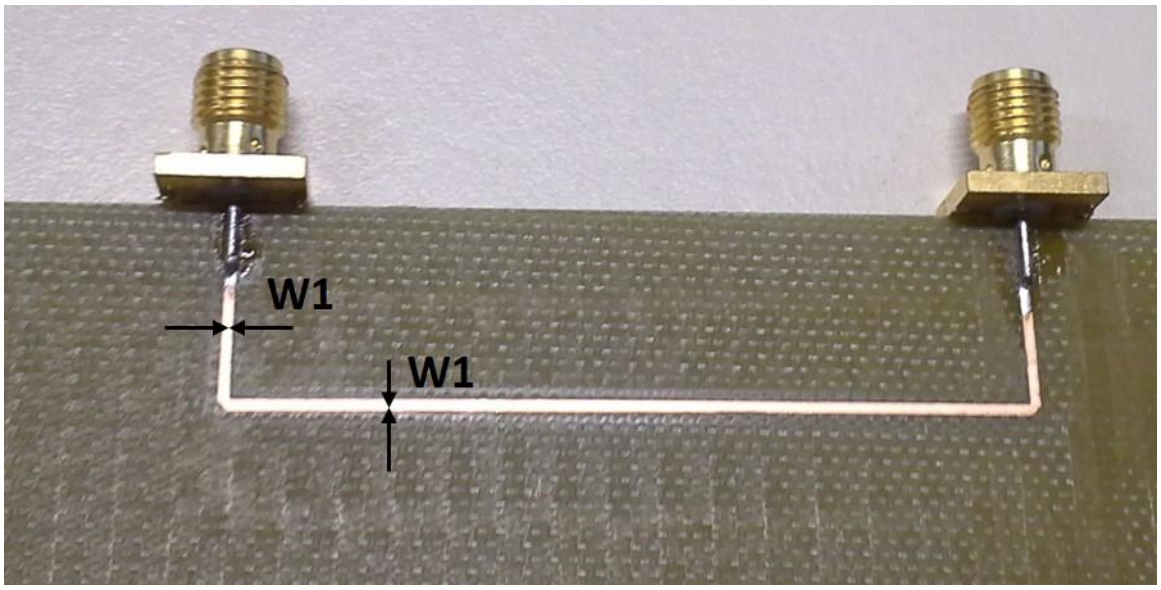

(a) U design

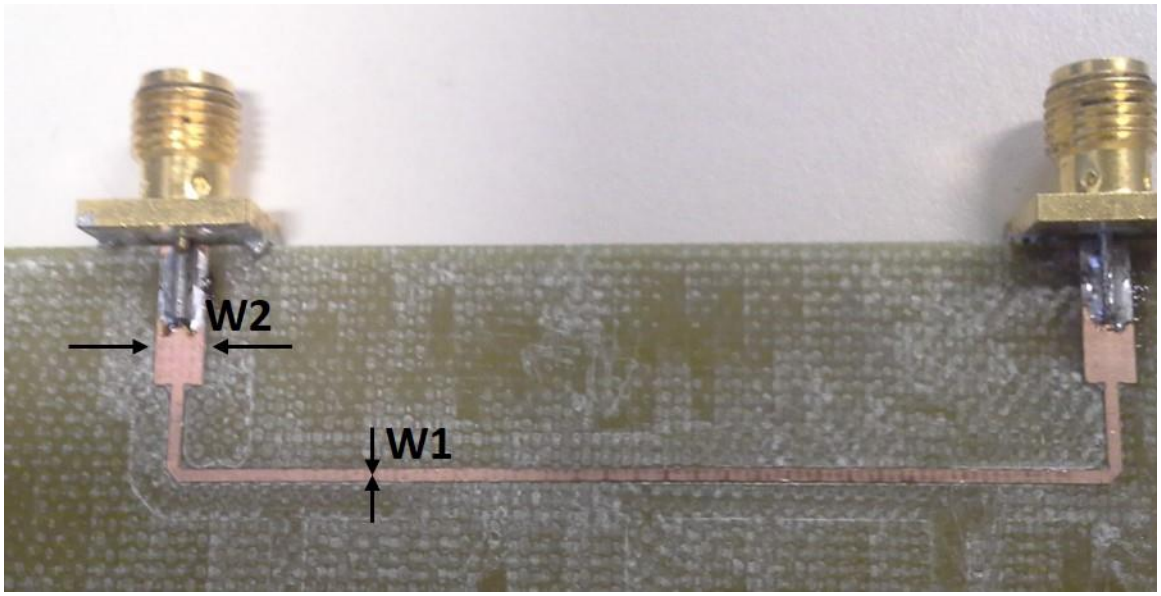

(b) T design

Figure 2.6. The design (a)-without transition (U) (b) with transition (T) for DI H_2O as the superstrate

Two different calibration levels is used for testing the liquid: partial submersion-P/S and complete submersion-C/S. For the transition design-T (Fig. 2.4(b)), the W1/W2 transition serves as a liquid placement marker to set the level of the liquid to be measured as seen in Fig. 2.7(a), hence partial submersion is used. For the uniform design-U (Fig.

2.4(a)), there is no transition hence, both partial submersion and complete submersion is possible. The two uniform cases are shown in Fig. 2.7 (b) and (c).

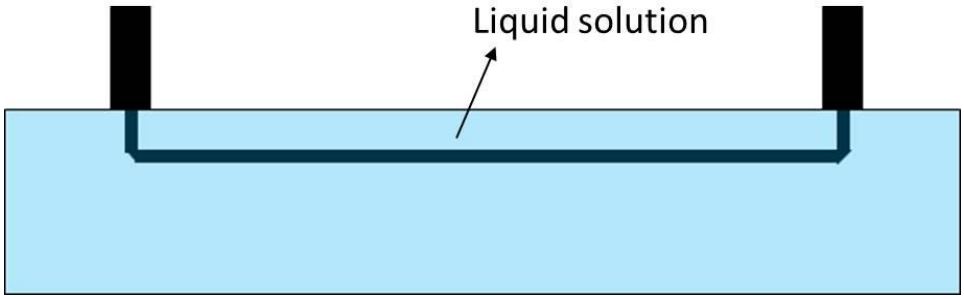

(a) T (with transition) with PS (Partial Submersion)

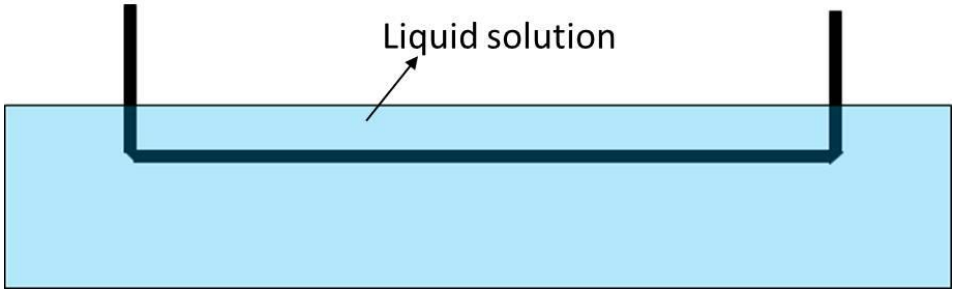

(b) U (no transition) with PS (Partial Submersion)

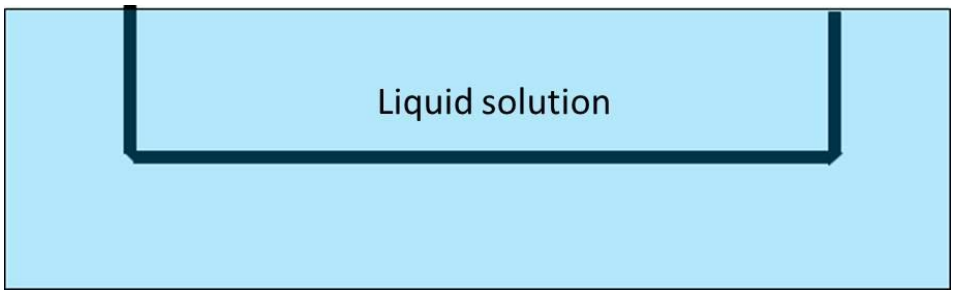

(c) U (no transition) with CS (Complete Submersion)

Figure 2.7:- Calibration lines for different designs:- (a) T(with transition) with PS(Partial Submersion) (b) U(no transition) with PS(Partial Submersion) (c) U(no transition) with CS(Complete Submersion)

For DI H_2O there are 3 options to choose from T/PS, U/PS and U/CS. For FC40 there are 2 options U/PS and U/CS. The goal of this section is to show that for DI H_2O, T/PS (transition with partial submersion) is the best design and for FC40, U/PS (uniform

with partial submersion) is the better design. To analyze these designs and liquid levels, S parameter data collection is obtained using an Anritsu 37369D Network Analyzer, and calibrated using the standard SOLT calibration technique. The microstrip transmission line was then connected to the network analyzer and placed in the beaker. Liquid is poured into the beaker. The amount of fluid was always adjusted to either reach the transition level for partial submersion or just cover the top of the microstrip line without contacting the barrel end of the SMA connectors for complete submersion. The network analyzer was then used to calculate the S-Parameter data on the circuit.

Figure 2.8 a and b shows the |S11| and |S12| for DI H_2O, using the 3 designs (T/PS, U/PS and U/CS) that are represented by 3 curves in the graph. It can also be seen that the design T/PS gives the best consistent matching to the SMA in lossy fluids like DI H_2O. It is hence concluded that the match is better with a short section of microstrip (T/PS), to allow for the conversion of the coaxial mode (SMA) to microstrip mode before evaluating the fluid system. The |S12| is very low, thus showing that DI H_2O is very lossy.

Figure 2.9 shows the |S11| and |S12| for the uniform line for the 2 designs (U/PS and U/CS) for the FC40 medium. The additional line length submerged in the complete submersion case (U/CS) add to the loss of the entire system hence making |S12| lower. The |S11| is almost the same, as the dielectric constant of FC40 is close to air.

In conclusion the length of the line submerged in the liquid affects the matching and the losses observed in the S parameters. For DI H_2O the T/PS (transition with partial submersion) gives the best matching whereas, with FC40 the U/PS shows lower losses as compared to U/CS.

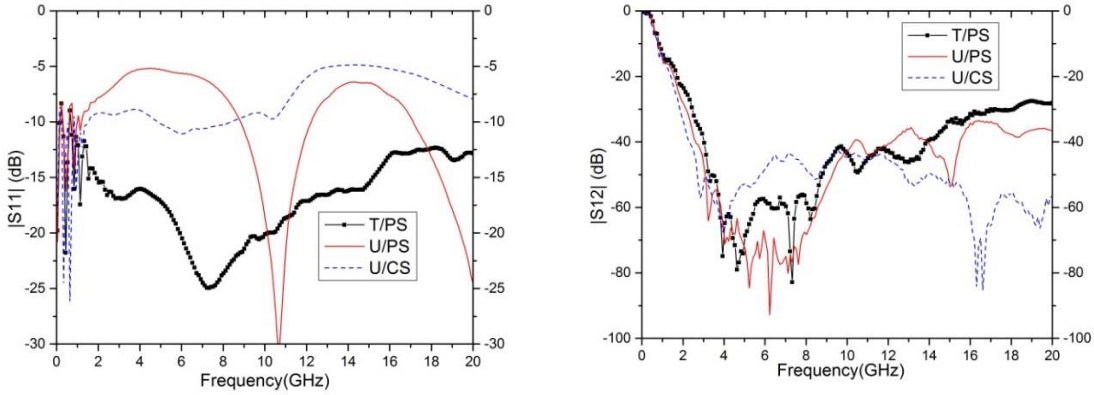

(a) (b)

Figure 2.8. Magnitude of (a) S11 and (b) S12 of the fabricated circuit in Fig. 2.6 a and b for DI H_2O. The 3 curves represent transition with partial submersion (black), uniform with partial submersion of FC40 (red) and uniform with complete submersion (blue).

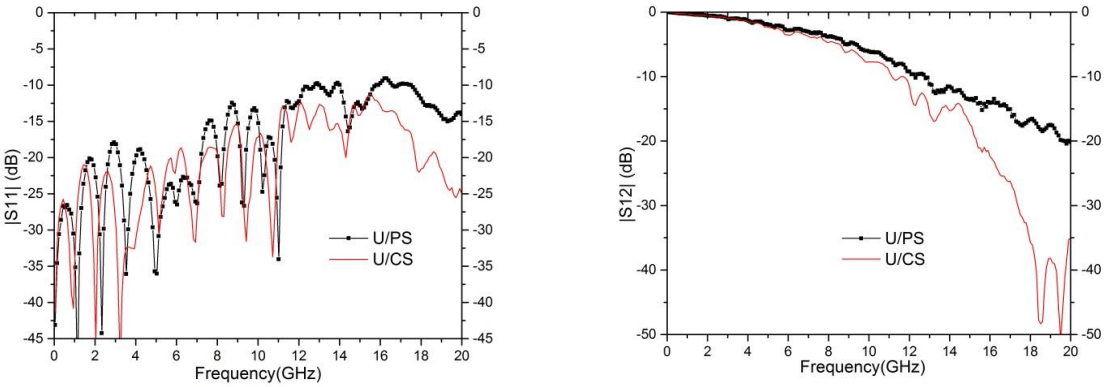

(a) (b)

Figure 2.9. Magnitude of (a) S11 and (b) S12 of the fabricated circuit in Fig. 2.5 for FC40. The 2 curves represent partial submersion(black) and complete submersion of FC40(red) liquid

2.3 Design Algorithm for the Fluid Microstrip Lines

The design of the Microstrip T-Line is performed using LineCalc in ADS 2011 Software [20]. The microstrip design is described in the layout shown in Fig. 2.1. It is implemented on FR4 PC board (ε_r=4.78 and tanδ=0.015) for substrate thickness of 60 mils and conductor thickness of 1.4 mil copper. The lines are designed to be matched to 50 ohms for the different superstrate sections of line. Since LineCalc models the conventional

microstrip substrate environment (air above the conductor, substrate below the conductor), an algorithm is required, that combines static equations and LineCalc to produce the appropriate transmission line design that accounts for the non-air behavior of the fluids that will reside on top of the conductors in the fluid test cases. A flow chart is shown in Appendix A that describes the algorithm used to design the u-line section submersed in the fluid.

The flowchart in Appendix A uses the microstrip standard equation (Eq A.1) [19] to find the effective dielectric constant for the given medium. It then, uses this effective dielectric constant to find out the value of dielectric constant for the substrate, given that the medium is air. These values are obtained through quasi static equations. LineCalc ADS has frequency dependent equations, the resultant values are entered into LineCalc which uses the frequency dependent equation for microstrip design. The dielectric constant of the board is changed till the effective dielectric constant (εeff achieved using the equation A.1) and Z_0=50 Ω is achieved.

Lines with different electrical lengths were designed for each surrounding medium to eliminate the irregularities and discontinuities due to SMA connectors and the chamfered edges at the corners as seen in Fig. 2.5 & 2.6. Table 2.1 has the results from the algorithm for mediums with different dielectric constant. Measured dimensions of the board using Vernier calipers are shown in Table 2.2. The depth of the board was around 55 to 56.2 mils. The deviation from the designed values was due to the milling machine error tolerance.

It should be noted that the frequency dependence of the dielectric constant and loss of the liquid was not considered while designing the line. For example, dielectric constant and loss for DI H_2O at 3 GHz is 76 and 0.1454 respectively, whereas, at 15 GHz it is 50.71 and

0.6972 respectively[22,23]. Hence the line width obtained will be matched for a small frequency range. For the values obtained in Table 2.1 Dielectric constant of 80 is used for DI H_2O.

Table 2.1. Microstrip Line physical dimensions for air, DI H_2O and FC40 as surrounding mediums, derived from the flowchart

Surrounding Medium	Air, FC40 long, short	DI H_2O long, short
Dielectric constant range	<5	>30
Electrical length (degrees)	1984.94,1673.81	6104.05, 5258.23
Width(w) (mils)	108.75	27.025
Length (mils)	3317.5,2797.5	3154.05, 2629
Impedance in air (Ω)	50	95

Table 2.2. Microstrip Line measured dimensions for air, DI H_2O and FC40 as surrounding mediums.

Surrounding Medium	Air, FC40 long, short	DI H_2O long, short
Width(w)(mils)	108	28
Length(mils)	3319,2788.5	3160,2636

2.4. Testing and Calibration to Extract Dielectric Constant

The circuit designed and tested in this section can be used to find the relative permittivity of a dielectric superstrate using equations 2.1 and 2.2. In these two equations: εr is the relative permittivity of substrate (FR4 Board), εf is the relative permittivity of superstrate (fluid), εeff is the effective permittivity of circuit. In equation 2.1, d is the height of the substrate and w is width of the Microstrip. In equation 2.2, ϑ_l & ϑ_s is the measured unwrapped S12 phase of the circuit for the long line and short line respectively, c is the velocity of light, f is the discrete frequency of each data point, l_l and l_s is the length of the line measured in meters for the long line and short line respectively.

$$\varepsilon eff = \frac{\varepsilon r + \varepsilon f}{2} + \frac{\varepsilon r - \varepsilon f}{2\sqrt{1 + 12\,(\frac{d}{w})}} \qquad \text{Eq 2.1}$$

$$\varepsilon eff = (\frac{(\vartheta_{l(rad)} - \vartheta_{s(rad)}) * c}{2\pi f(l_l - l_s)})\text{^}2 \qquad \text{Eq 2.2}$$

The data collection is obtained using an Anritsu 37369D Network Analyzer, and calibrated using the standard SOLT calibration technique. The detailed procedure of the calibration and measurement is described in Appendix C. The long Microstrip transmission line is then connected to the network analyzer and placed in the beaker. Approximately 2.5 liters of fluid is then poured into the beaker. The amount of fluid is always adjusted to just reach the transition between the feedline and transmission line. The network analyzer is then used to calculate the S-Parameter data on the circuit. This data is ultimately used to produce relative permittivity using the equations discussed in this section. After the measurements, the long Microstrip line is replaced with the short Microstrip line and the entire process is repeated to produce the new set of S parameter data. The εeff is calculated from the processed phase difference and lengths of the line using Eq 2.2. This calculated εeff is then used to extract the εf of the liquid using Eq 2.1. The extraction procedure for microstrip is discussed more in Appendix B.

The plot of relative permittivity of FC40 calculated using this technique is seen in Fig. 2.10. FC40 being low loss liquid, the dielectric constant extracted through this method is close to the dielectric constant of 1.9. The graph shows slight variation in the entire

frequency range but it is around 1.9 in the X band range. The DI H_2O plot shows a lot of variation with frequency as seen in Fig. 2.11, this is attributed to the high loss in the liquid.

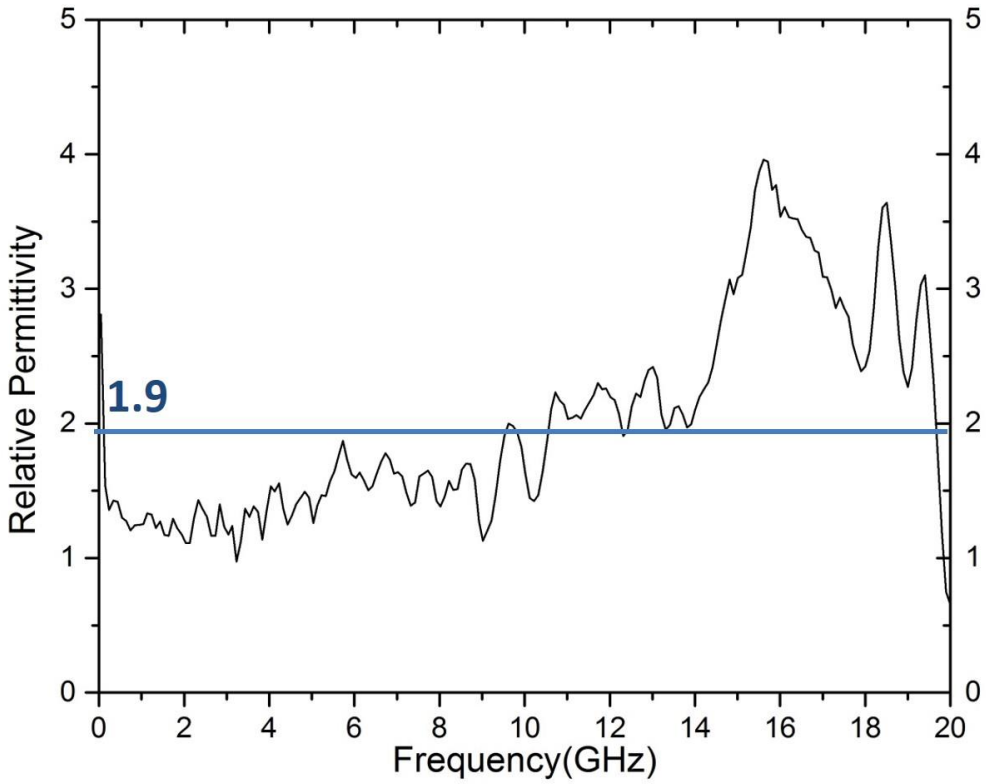

Figure 2.10: Plot of relative permittivity of FC40

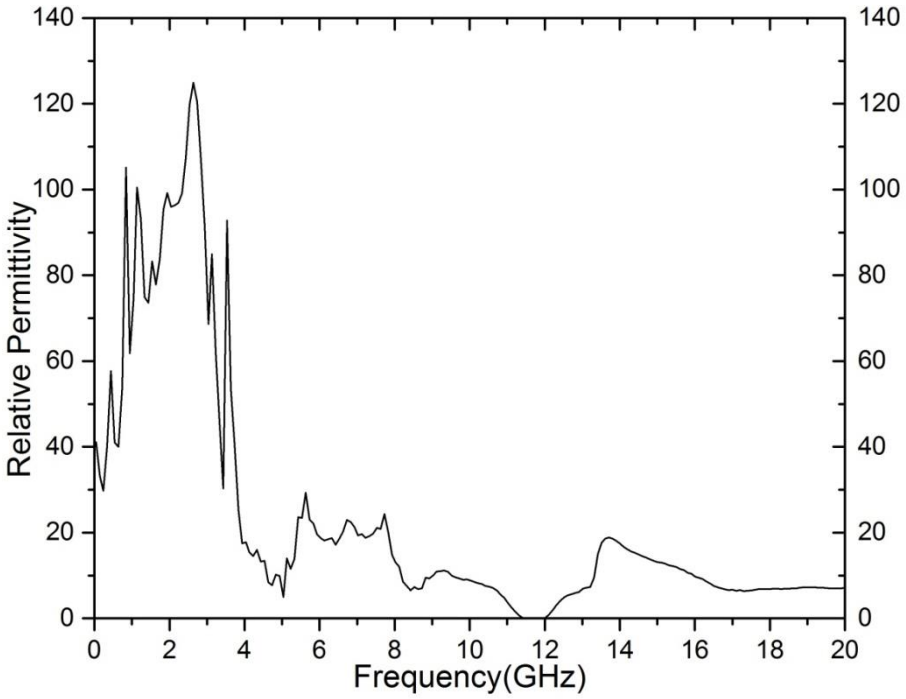

Figure 2.11: Plot of relative permittivity of DI H_2O

The dielectric loss attenuates the signal (S21) further thereby making the propagation constant a complex quantity. In the algorithm to extract the dielectric constant, the propagation constant is assumed to be imaginary. Moreover, the microstrip test structure design does not factor in the change in dielectric constant of DI H_2O with frequency. This change cannot be ignored, hence the matching is not effective. To analyze high loss liquids the frequency is restricted to 3 GHz.

2.6 Conclusions

High dielectric constant liquids have high loss which attenuates the signal, thereby making it inefficient for use in tuning RF circuits. Low dielectric constant liquids does not

provide with a good tuning range. A compromise is made with either loss or tuning range. The extraction algorithm in this section is for low loss liquids such as FC40. For high loss liquids such as DI H_2O and Ethylene Glycol, the analysis will be restricted from dc to 3 GHz.

CHAPTER 3

TEMPERATURE STUDY OF FLUIDS USING COPLANAR WAVEGUIDE

3.1 Introduction

As seen in Fig. 2.8(a) and (b), the microstrip line with transition and partial submersion gives the best matching and provides better transmission than the other designs. There has been extensive work done on using coplanar waveguides for dielectric spectroscopy [13], [24-27]. To design the coplanar waveguide, the same algorithm mentioned in Section 2.3 and described in Appendix A is used to extract the microstrip line impedance. Using this impedance and line calc (ADS [20]) the width of the trace and gap was synthesized for the coplanar waveguide. The schematic of the coplanar waveguide is seen in Fig. 3.1. The analysis of RF electrical properties of liquids with heat is a relatively unexplored area of research. In [28] a dielectric probe and E Cal software is used to extract the change in dielectric properties of water from 100 MHz to 20 GHz with the temperature varying from 0^0C to 90^0C. In this work using coplanar waveguide test structure, an attempt is made to analyze dielectric constant bulk liquids in the RF domain (X Band).

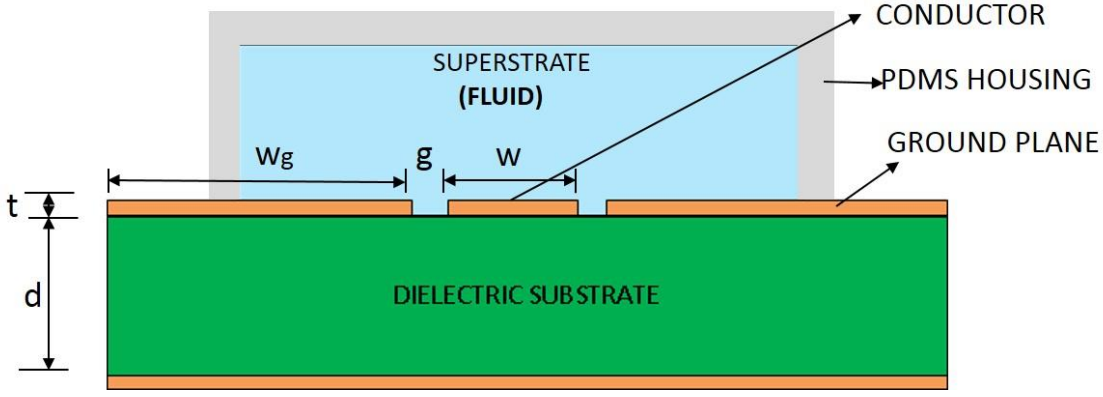

Figure 3.1:- Schematic of the coplanar waveguide without ground back plate. Wg=3(S+W) to ensure that the stripline mode is not excited.

3.2. Design of the Coplanar Waveguide Apparatus to Test the Fluid RF Behavior

The physical circuit layout is designed to allow the line to be submerged in the fluid under test and isolate the leads of the Network Analyzer from the fluid, identical to the Microstrip Line test structure. See Appendix D for more details on the measurement setup and procedure. This design is documented in Fig. 3.2. All designs (TLine and substrate structure) use the layout tool in ADS to create an exported file that is fed to a computer controlled LPKF PhotoMat C60 Milling Machine.

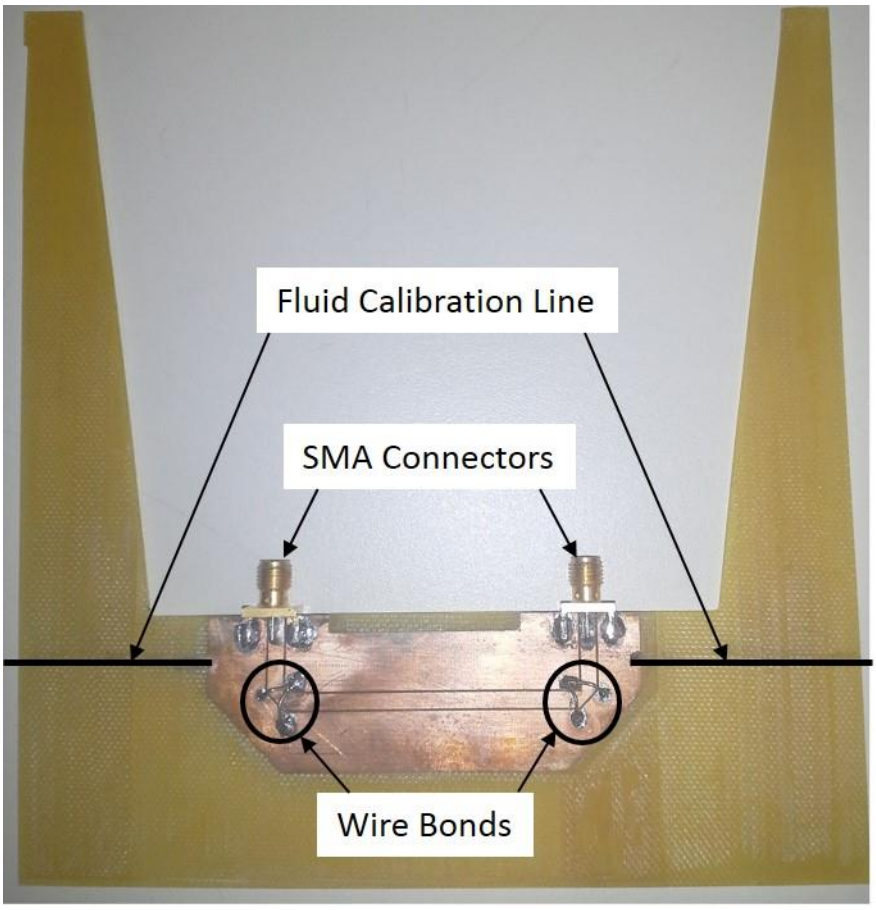

(a) Coplanar waveguide placement on the substrate

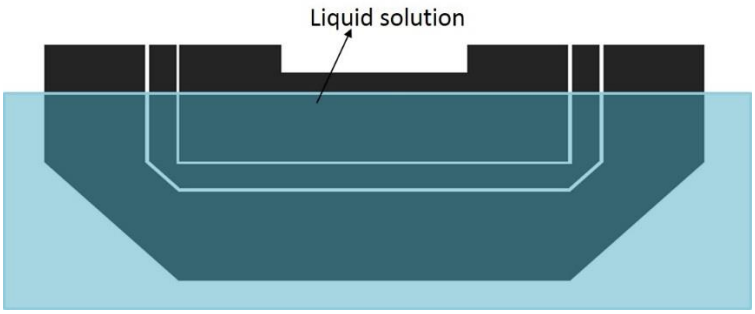

(b) Liquid placement relative to the coplanar waveguide

Figure 3.2 (a). Coplanar waveguide system design. The approximate placement of coplanar waveguide relative to the substrate is shown here.(b) liquid placement relative to the coplanar waveguide is also seen here.

3.3. Design of Specific Coplanar Waveguide Test Circuits for Fluid Characterization

Using the conclusions drawn for the design in the microstrip test cases, uniform line with partial submersion (U/PS) is used for FC40 (any $\varepsilon_r<5$) and transition line with partial submersion (T/PS) is used for DI H_2O (any $\varepsilon_r > 30$). An additional design constraint is added to the coplanar waveguide design, with or without the back ground plane. For FR4 the U/PS is used without ground plane as seen in Fig. 3.2(a). For DI H_2O, the T/PS with (wbp) and without (wobp) ground plane is used to determine the optimum design as seen in Fig. 3.3(a) and (b). Given that the resolution of the milling machine was 5 mils, the design parameters for materials with dielectric constant greater than 30 converged. Thus, a single design board could be used for ethylene glycol (37.7) [11], DI H_2O (80) [10], 50% mixture ($37.7 < \varepsilon r < 80$) [23]. FC40 ($\varepsilon r=1.9$) [12] has dielectric constant close to air, thus the uniform design was sufficient. Lines with different electrical lengths were designed for each surrounding medium to eliminate the irregularities and discontinuities due to SMA connectors and the chamfered edges at the corners. The design physical dimensions are listed in Table 3.1 for the 3 design configurations.

Table 3.1. Coplanar Waveguide design physical dimensions for low and high εr as surrounding medium, derived from the algorithm (Appendix A) and Line Calc at 10 GHz			
Design	Uniform(U) long, short	Transition with back plate(wbp) long, short	Transition without back plate(wobp) long, short
Dielectric constant range	<5	>30	>30
Width W (mils)	108.75	23	39
Spacing S (mils)	13.76	67.85	48.4
Length (mils)	3317.5, 2797.5	3317.5, 2797.5	3317.5, 2797.5

For the case of DI H_2O as seen in Fig. 3.3, the narrow line (23 mils (wbp) and 39 mils (wobp)) with air above the conductor produces an impedance of 95 ohms but it produces an impedance of 50 ohms with DI H_2O. The wider line (108.75 mils) produces an impedance of 50 ohms in air as seen in Fig. 3.3.

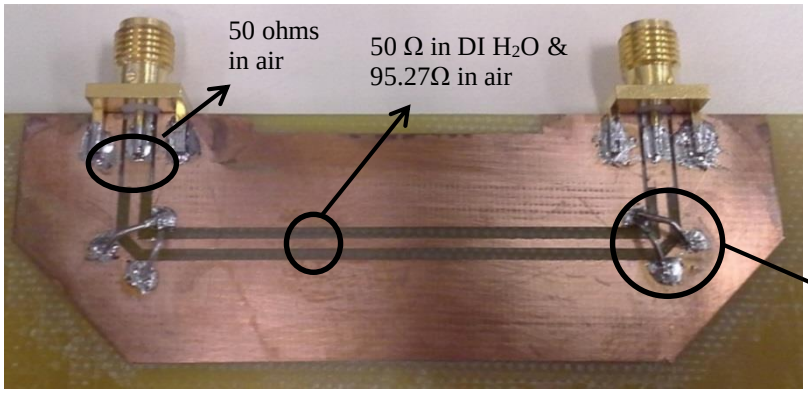

(a) Coplanar waveguide without back plate for solutions with dielectric constant above 30. The thicker trace line with smaller gap is 50 ohms in air and the thinner line with wider gap is 95.27 ohms in air and 50 ohms in DI H_2O or any solution with $\varepsilon r > 30$.

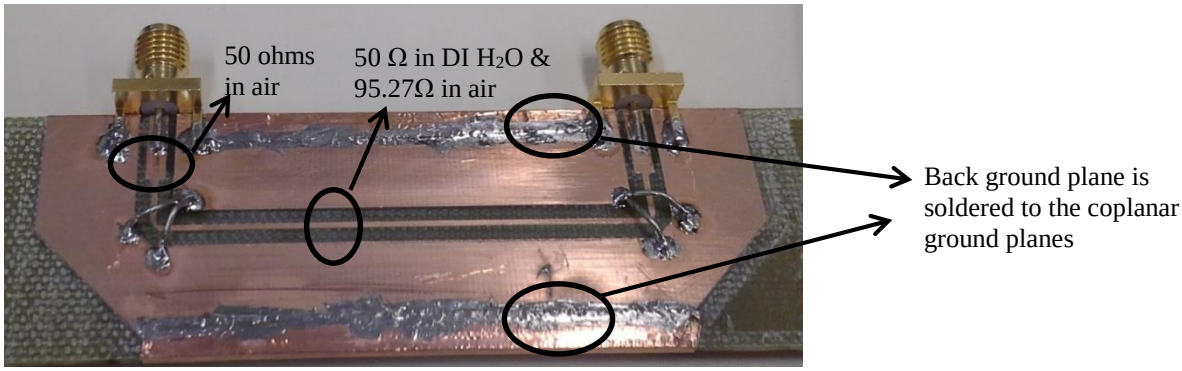

(b) Coplanar waveguide with back plate for solutions with dielectric constant above 30. The thicker line is 50 ohms in air and the thinner line is 95.27 ohms in air and 50 ohms in di water or any solution with er > 30.

Figure 3.3:- The wbp and wobp boards with the wirebonds for DI H_2O as the surrounding medium (or any material with ε_r greater than 30)

The reason for using coplanar waveguide henceforth, as the test structure for heat analysis is seen in Fig. 3.4 & 3.5. A comparison of S11 and S12 of microstrip and coplanar waveguide structure for DI H_2O and FC40 is shown in Fig. 3.4 and 3.5 respectively. It was determined that the match is better for the case with the back plate for solution with dielectric constant greater than 30 as shown in Fig. 3.4. There is a 30% improvement in the losses for the cpw_wbp when compared to cpw_wobp and microstrip. The losses are lower for the cpw _U than the microstrip line when the liquid is FC40.

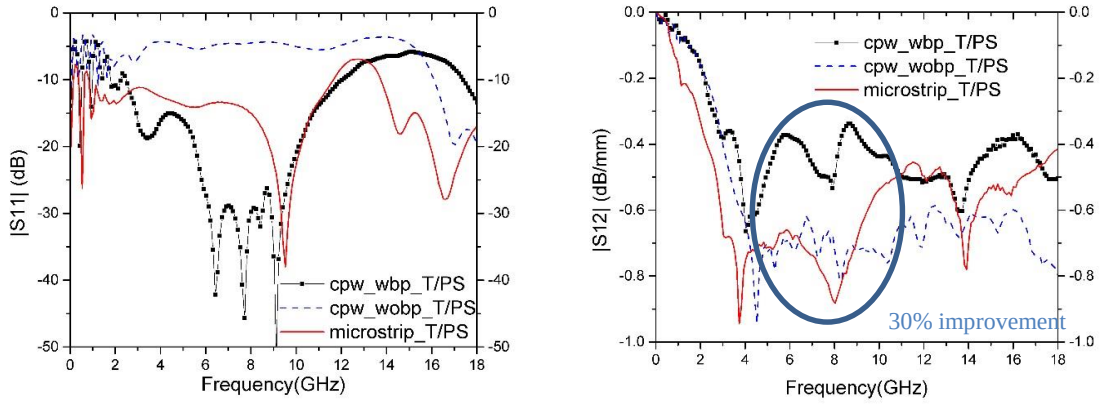

(a) (b)

Figure 3.4. Magnitude of S11(dB) and S12(dB/mm) of the short coplanar waveguide (2797.5 mils) for a comparison with the microstrip_T/PS , cpw_wbp_T/PS & cpw_wobp_T/PS with DI H_2O as the superstrate

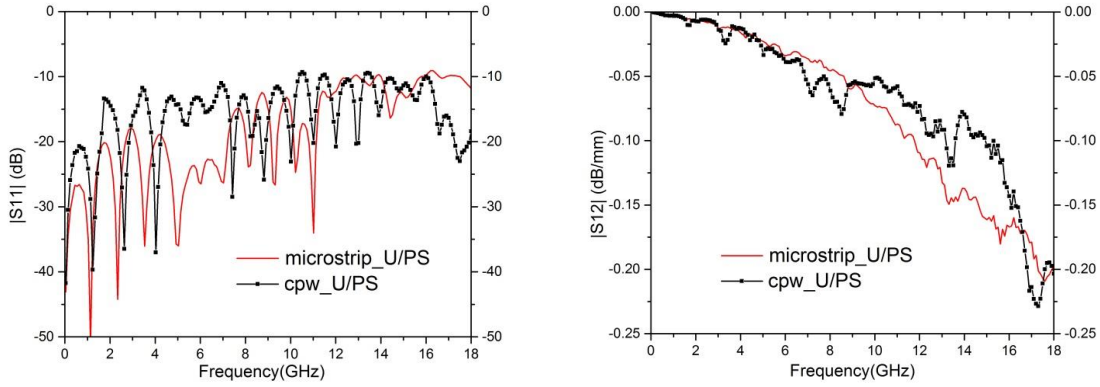

(a) (b)

Figure 3.5. Magnitude of S11(dB) and S12(dB/mm) of the short coplanar waveguide (2797.5 mils) for a comparison with the microstrip_U/PS & cpw_U/PS withfor FC40 as the superstrate

3.4 Testing and Calibration to Extract Dielectric Constant

The circuit designed and tested in this section can be used to find the relative permittivity of a dielectric superstrate using equations 3.1, 3.2 and 3.3 [29-32]. In these two equations: εr is the relative permittivity of substrate (FR4 Board), εf is the relative permittivity of superstrate (fluid), εeff is the effective permittivity of circuit. In equation 3.1, ϑ_l & ϑ_s is the measured unwrapped S12 phase of the circuit for the long line and short line respectively, c is the velocity of light, f is the discrete frequency of each data point, and l_l and l_s is the length of the line measured in meters for the long line and short line respectively. In equation 3.2 & 3.3, K(k) and K'(k) are the complete elliptical integrals of the first kind.

$$\varepsilon eff = \left(\frac{\left(\vartheta_{l(rad)} - \vartheta_{s(rad)}\right) * c}{2\pi f(l_l - l_s)}\right)\text{^}2 \qquad \text{Eq 3.1}$$

Coplanar Waveguide without ground plane

$$\varepsilon eff = \varepsilon f + \frac{\varepsilon r - \varepsilon f}{2} \frac{K(k2)}{K'(k2)} \frac{K'(k1)}{K(k1)} \quad \text{Eq 3.2}$$

Where

$$C = \frac{K(k2)}{K(k2)} \frac{K'(k1)}{K(k1)}$$

,

$$k_1 = \frac{a}{b} \sqrt{\frac{1-\frac{b^2}{c^2}}{1-\frac{a^2}{c^2}}} \quad , k_2 = \frac{\sinh\left(\frac{\pi a}{2d}\right)}{\sinh\left(\frac{\pi b}{2d}\right)} \sqrt{\frac{1-\sinh 2\left(\frac{\pi b}{2d}\right)\sinh 2\left(\frac{\pi c}{2d}\right)}{1-\sinh 2\left(\frac{\pi a}{2d}\right)\sinh 2\left(\frac{\pi c}{2d}\right)}}$$

a = W/2, b=W/2+S, c=W/2+S+Wg

Coplanar Waveguide with ground plane

$$\varepsilon eff = \varepsilon f \frac{B}{A+B} + \varepsilon r \frac{B}{A+B} \quad \text{Eq 3.3}$$

where $A=K(k_3)/K'(k_3)$ & $B=K(k_4)/K'(k_4)$

$$k_3 = \frac{a}{b} \sqrt{\frac{1-\frac{b^2}{c^2}}{1-\frac{a^2}{c^2}}} \quad , \quad k_4 = \frac{\tanh\left(\frac{\pi a}{2d}\right)}{\tanh\left(\frac{\pi b}{2d}\right)}$$

a = W/2, b=W/2+S, c=W/2+S+Wg

The data collection is obtained using an Anritsu 37369D Network Analyzer, and calibrated using the standard SOLT calibration technique. After calibration, the device is never recalibrated or turned off until all the tests are completed. To test each fluid, a 4 liter beaker was set on a hotplate. A magnetic stir bar is placed in the bottom of the beaker. A thermometer is placed in the beaker to monitor the temperature of the fluid during testing. Approximately 2 liters of fluid is poured into the beaker. The long cpw of length 3317.5 mils is then connected to the network analyzer and using the adjustable clamps, is lowered into the beaker, till the liquid level reaches the calibration line. The complete setup with

fluid in the beaker and the clamps and the procedure can be seen in Appendix E. The network analyzer is then used to calculate the S-Parameter data on the circuit. After the measurements, the long cpw line of length 3317.5 mils is replaced with the short cpw line of length 2797.5 mils and the entire process is repeated to produce the same data with this line. The extraction algorithm that is used herein does not take into account the losses of the line and the medium (superstrate). The analysis will be restricted from dc to 3 GHz.

3.5. ANALYSIS OF DATA/RESULTS

Three different fluids are tested using this setup. The network analyzer is then used to acquire S-Parameter data on the circuit for the long line. After collecting S-Parameter data at room temperature for the long line, the short line is used to acquire the S parameter data. At every ten degrees between 25^0C and 105^0C, the procedure is repeated. Data is taken once the liquid's temperature is steady for at least 10 minutes. Temperature values for DI H_2O, ethylene glycol, 50% mixture solution by volume (50% DI H_2O and 50% ethylene glycol) and FC40 is shown in Table 3.2.

Table 3.2. Steady state temperatures achieved for DI H_2O, Ethylene Glycol, 50% mixture of DI H_2O + Ethylene Glycol & FC40

Liquid	Temperatures(^{0}C)
DI H_2O	23, 37, 46, 55, 65, 75, 82
Ethylene Glycol	24, 45, 55, 68, 76, 86, 94, 105
50% mixture solution	23, 37, 46, 55, 65, 75, 82
FC40	50, 65, 85, 105

3.5.1 Deionized Water (DI H_2O)

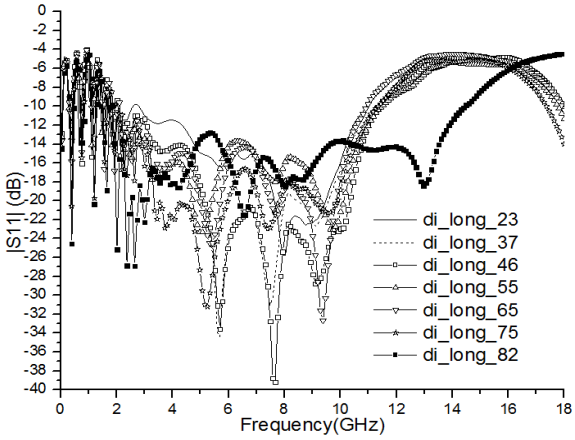

(a) Magnitude of S11 -long line

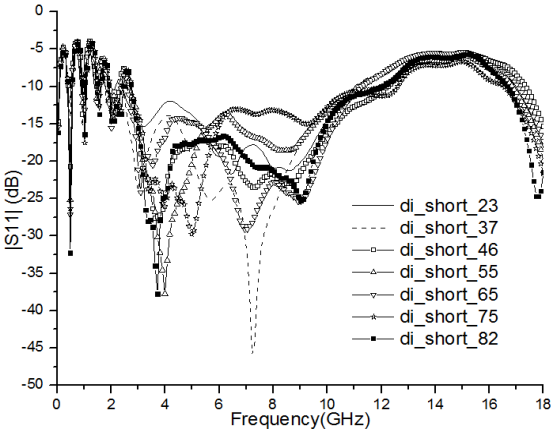

(b) Magnitude of S11 -short line

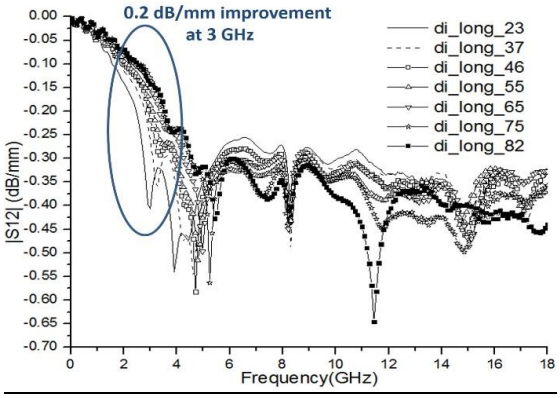

(c) Magnitude of S12 –long line

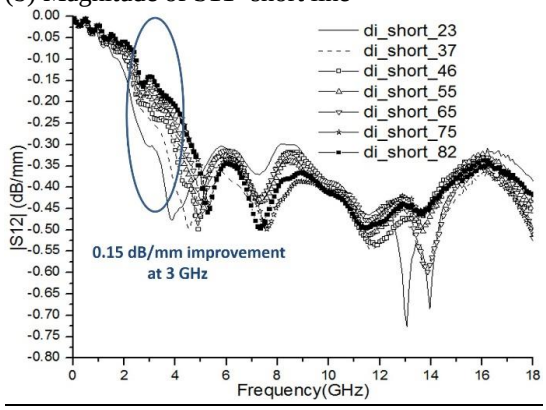

(d) Magnitude of S12 -short line

Figure 3.6:- Magnitude of S11 and S12 for the long and the short line for DI H_2O. The steady state temperatures are 23^0C, 37^0C, 46^0C, 55^0C, 65^0C, 75 ^{0}C and 82 ^{0}C. The legend for each curve represents di_long/short_ temperature.

The losses are expressed in dB/mm. The total length of the line is used to compute the losses per unit length. As highlighted above, losses seem to reduce with increase in temperature till about 3 GHz. After 3 GHz the losses get high enough to give inaccurate results with this loss free analysis/extraction.

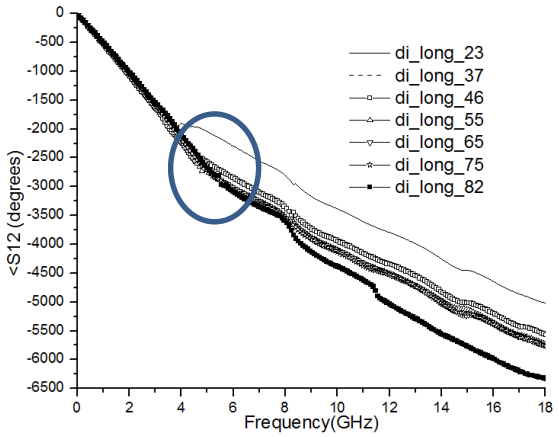

(a) Phase of S12- long line

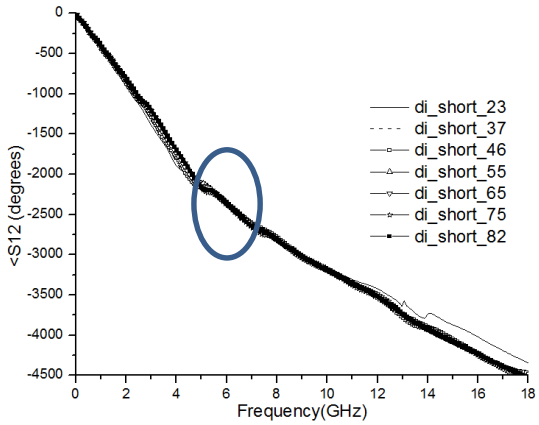

(b) Phase of S12- short line

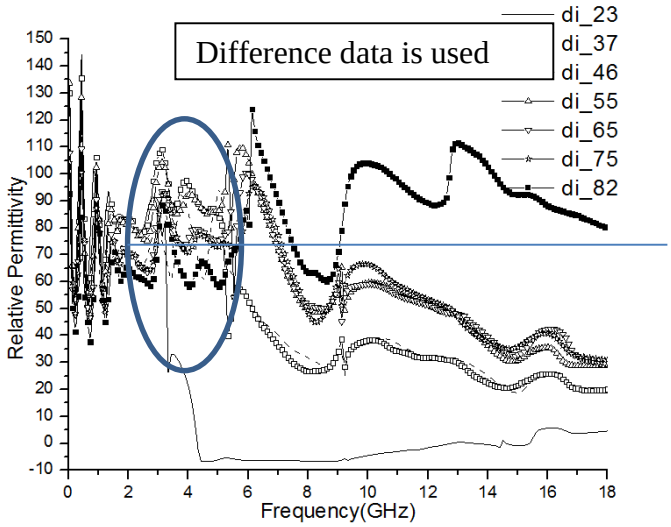

(c) Relative Permittivity- the blue line represents the approximate relative permittivity of DI H_2O

Figure 3.7:- Phase of S12 for the (a) long (b) short lines and (c) relative permittivity for DI H_2O. The legend for each curve represents di_long/short_ temperature.

There is a shift in the slope of the curves after 3 GHz as seen in Fig. 3.7 (a) and (b). The curves get parallel and are not in the same phase with increase in temperature. The relative permittivity extraction uses loss free analysis and hence the curves fail after 3 GHz as seen in Fig. 3.7 (c). Below 3 GHz with increase in temperature the extracted dielectric constant of the liquid decreases. The room temperature reading does not follow the trend. This can be attributed to the fact that there is no heat in the system at room temperature. So the liquid behaves differently with and without heat.

3.5.2 Ethylene Glycol

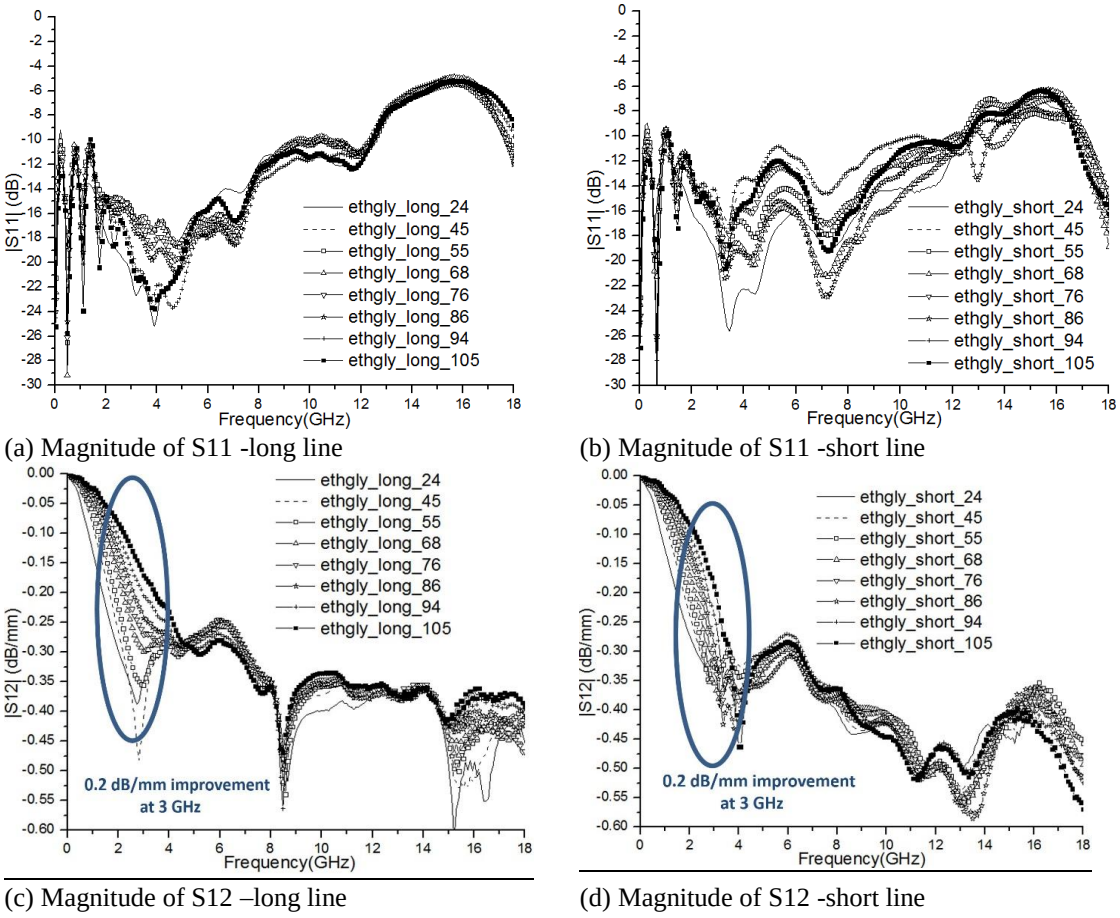

(a) Magnitude of S11 -long line

(b) Magnitude of S11 -short line

(c) Magnitude of S12 –long line

(d) Magnitude of S12 -short line

Figure 3.8:- Magnitude of S11 and S12 for the long and the short line for ethylene glycol. The steady state temperatures are 24^0C, 45^0C, 55^0C, 68^0C, 76^0C, 86^0C, 94^0C and 105^0C. The legend for each curve represents ethgly_long/short_ temperature.

The losses are expressed in dB/mm. The total length of the line is used to compute the losses per unit length. As highlighted above, losses seem to reduce with increase in temperature till about 3 GHz. After 3 GHz the losses get high enough to give inaccurate results with the loss free analysis/ extraction and therefore they do not follow the trend.

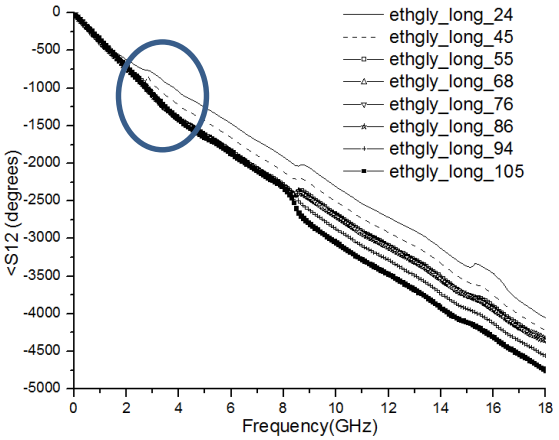

(a) Phase of S12- long line

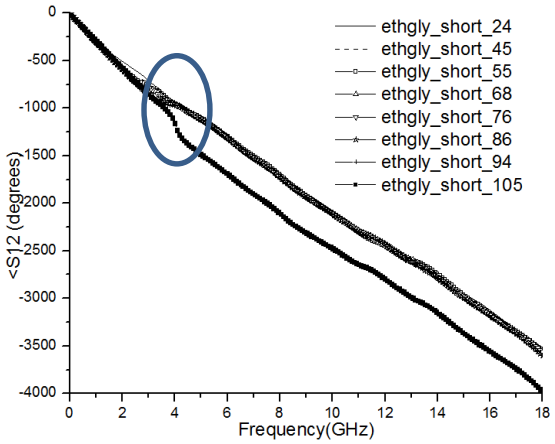

(b) Phase of S12- short line

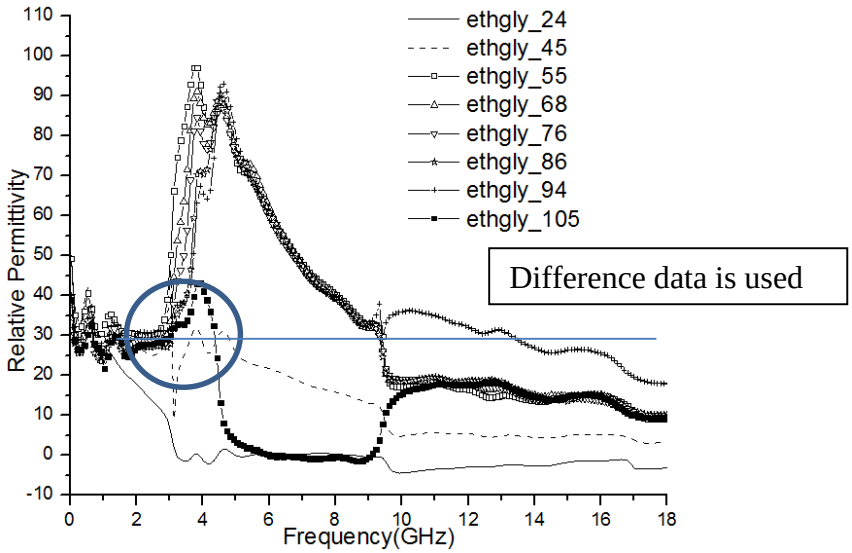

(c) Relative Permittivity- the blue line represents the approximate relative permittivity of the ethylene glycol

Figure 3.9:- Phase of S12 for the (a) long (b) short lines and (c) relative permittivity for ethylene glycol. The legend for each curve represents ethgly _long/short_ temperature.

There is a shift in the slope of the curves after 3 GHz as seen in Fig. 3.9(a) and (b). The curves get parallel and are not in the same phase with increase in temperature. The relative permittivity extraction uses loss free analysis and hence the curves fail after 3 GHz as seen in Fig. 3.9(c). Below 3 GHz the relative permittivity is fairly constant. The room temperature reading does not follow the trend. This can be attributed to the fact that there is no heat in the system at room temperature. So the liquid behaves differently with and without heat.

3.5.3. 50 % mixture by volume of DI H_2O and ethylene glycol

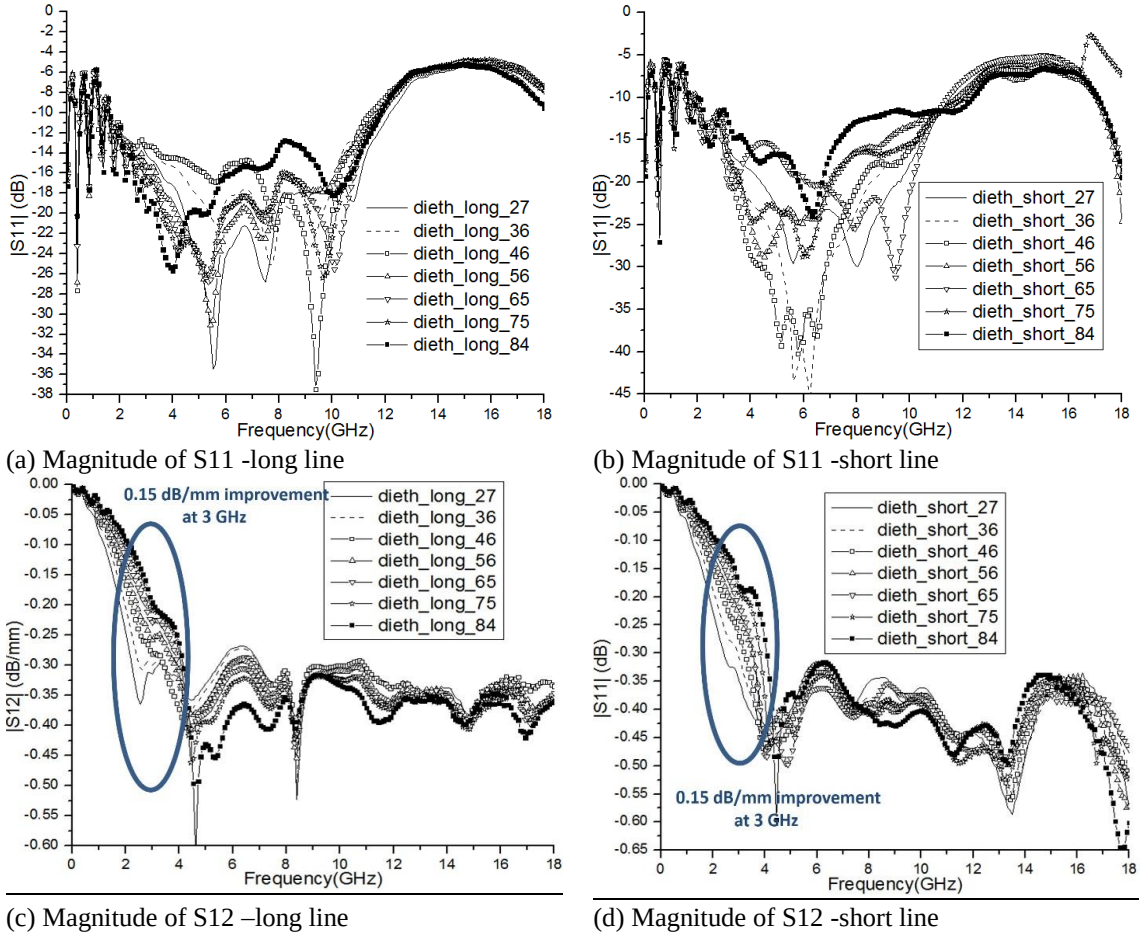

(a) Magnitude of S11 -long line

(b) Magnitude of S11 -short line

(c) Magnitude of S12 –long line

(d) Magnitude of S12 -short line

Figure 3.10:- Magnitude of S11 and S12 for the long and the short line for 50% mixture of DI H_2O and ethylene glycol. The steady state temperatures are 27^0C,36^0C, 46^0C, 56^0C, 65 ^{0}C,75 ^{0}C and 84 ^{0}C . The legend for each curve represents dieth_long/short_ temperature.

The losses are expressed in dB/mm. The total length of the line is used to compute the losses per unit length. As highlighted above, losses seem to reduce with increase in temperature till about 3 GHz. After 3 GHz the losses get high enough to give inaccurate results with the loss free analysis/ extraction and therefore they do not follow the trend.

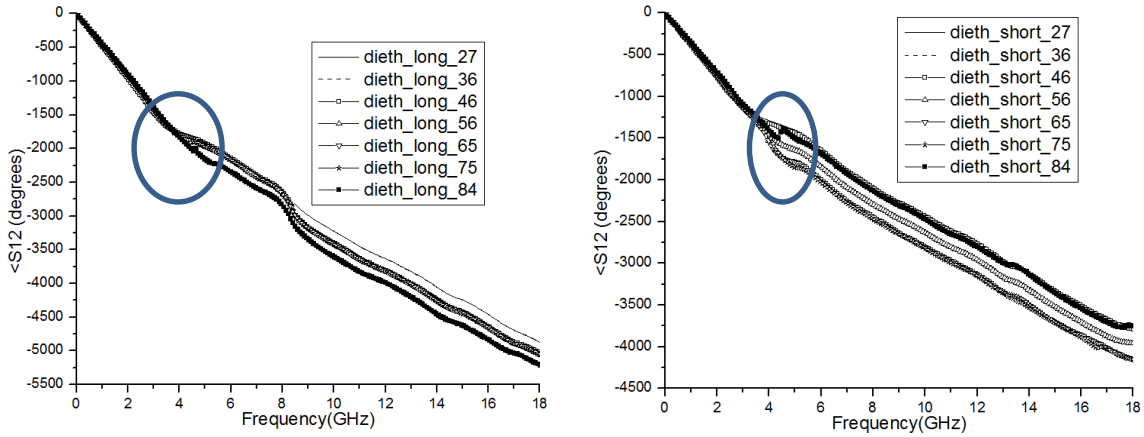

(a) Phase of S12- long line

(b) Phase of S12- short line

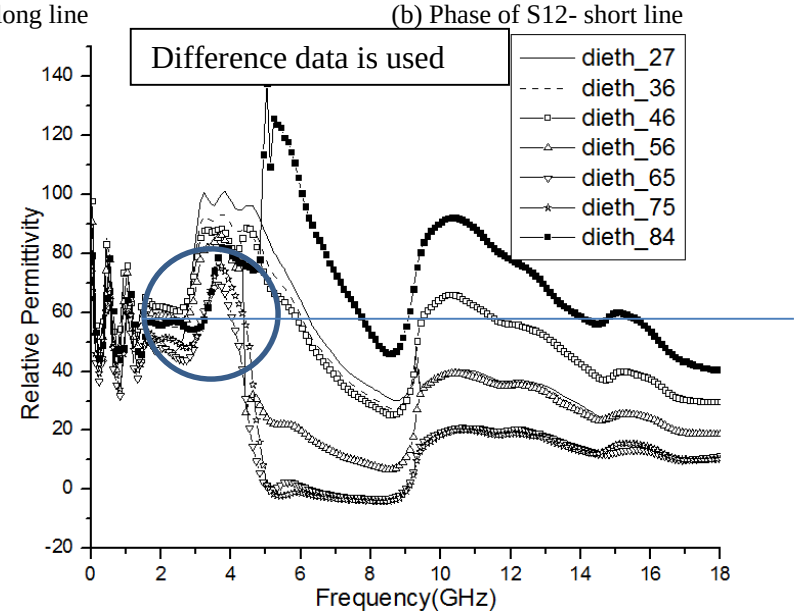

(c) Relative Permittivity- the blue line represents the approximate relative permittivity of the 50% mixture

Figure 3.11:- Phase of S12 for the (a) long (b) short lines and (c) relative permittivity for the 50% mixture DI H_2O and ethylene glycol. The legend for each curve represents dieth_long/short_ temperature.

There is a shift in the slope of the curves after 3 GHz as seen in Fig. 3.11(a) and 3.11(b). The curves get parallel and are not in the same phase with increase in temperature. The relative permittivity extraction uses loss free analysis and hence the curves fail after 3 GHz as seen in Fig. 3.11(c). Below 3 GHz with increase in temperature the extracted dielectric constant of the liquid decreases. The exact value of dielectric constant of the mixture is not known. The room temperature reading does not follow the trend. This can be attributed to

the fact that there was no heat in the system at room temperature. So the liquid behaves differently with and without heat. .

3.5.4 FC40

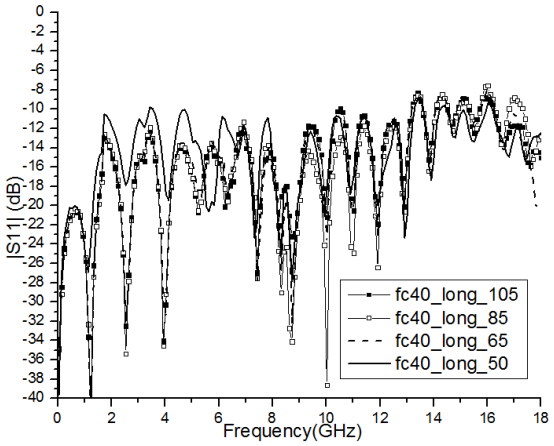

(a) Magnitude of S11 -long line

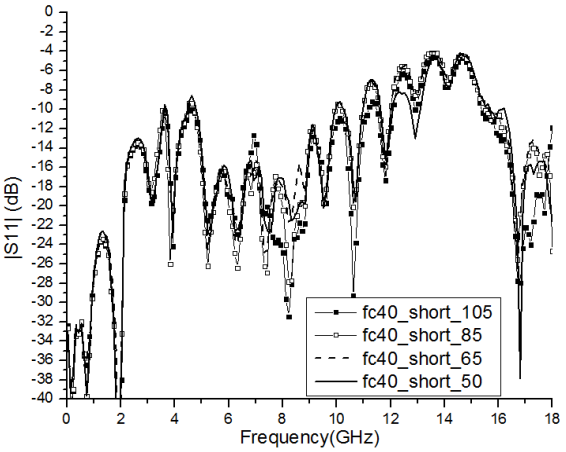

(b) Magnitude of S11 -short line

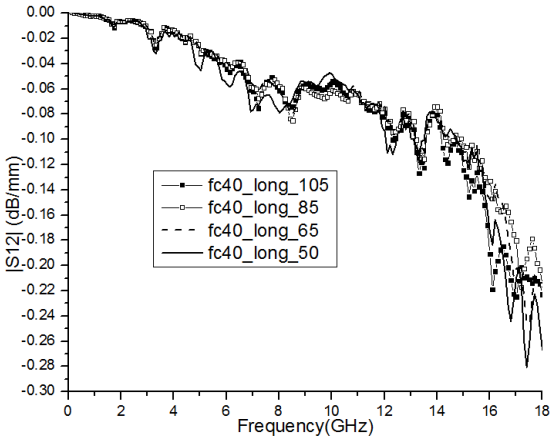

(c) Magnitude of S12 –long line

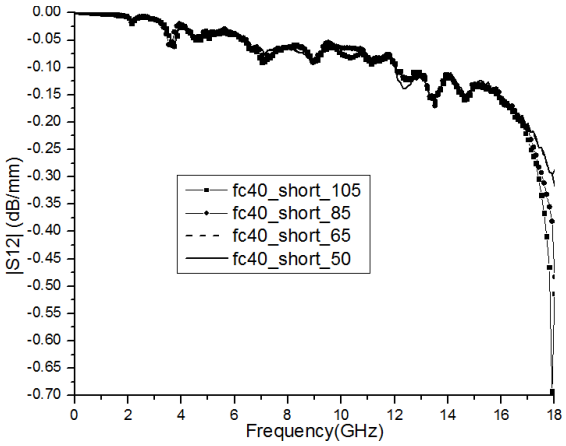

(d) Magnitude of S12 -short line

Figure 3.12:- Magnitude of S11 and S12 for the long and the short line for FC40. The steady state temperatures that were achieved were 50^{0}C, 65 ^{0}C,85 ^{0}C and 105 ^{0}C. The legend for each curve represents fc40_long/short_ temperature.

The losses are expressed in dB/mm. The total length of the line is used to compute the losses per unit length. The properties of the liquid do not change with temperature. They remain fairly constant with heating. This is due to the non-polar nature of the liquid. FC40 having low dielectric constant will not change its properties with increase in temperature.

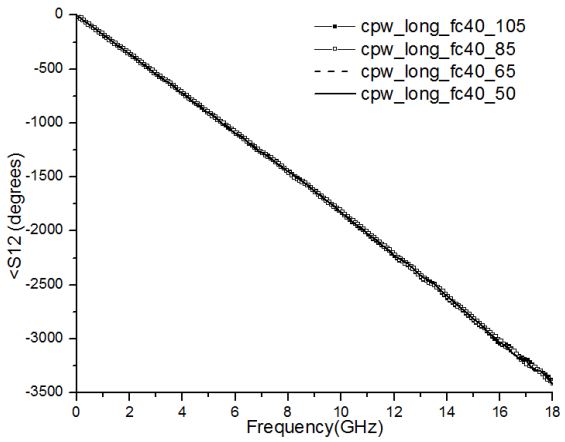

(a) Phase of S12- long line SOLT

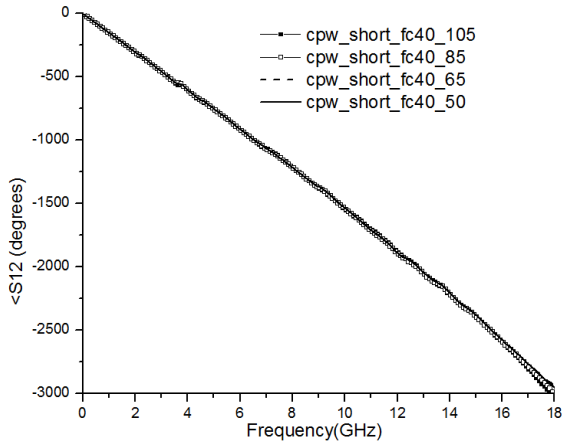

(b) Phase of S12- short line SOLT

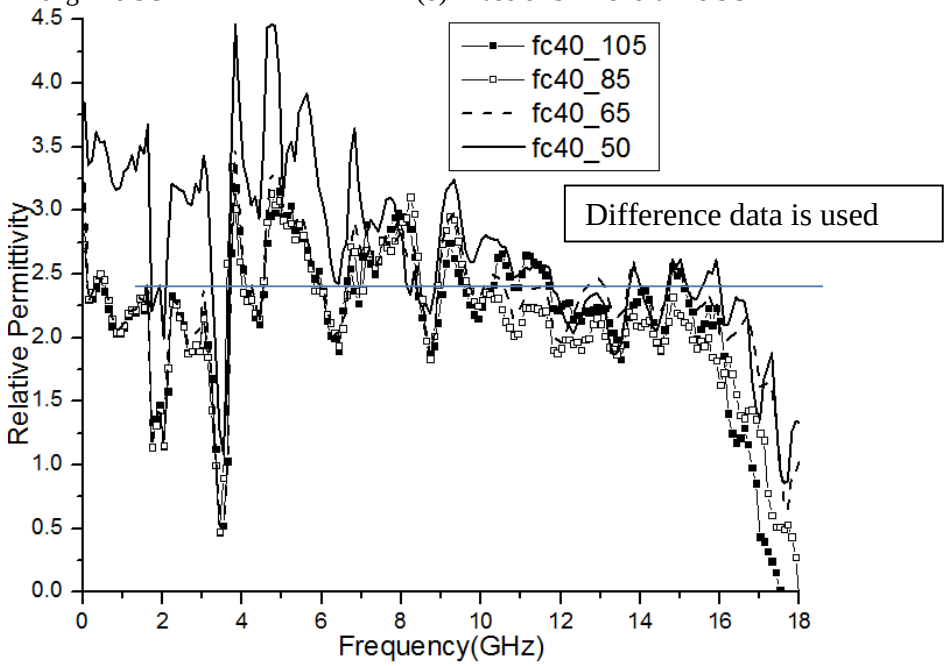

(c) Relative Permittivity- the blue line represents the approximate relative permittivity of FC40

Figure 3.13:- Phase of S12 for the (a) long (b) short lines and (c) relative permittivity for FC40. The legend for each curve represents fc40_long/short_ temperature.

The phase for all the curves overlap, again indicating that the properties of the liquid do not change with its temperature. The relative permittivity that is obtained is fairly close to the reltive permittivity of FC40. This analysis proves to be efficient with liquids that have low loss.

3.6. Conclusions

The 3 liquids DI H_2O, ethylene glycol and 50% mixture of DI H_2O and ethylene glycol are less lossy with increase in temperature as seen in the transmission data in the analysis. DI H_2O reduces loss by 0.3 dB/mm from room temperature of 25^0C to 82^0C. For ethylene glycol the losses have reduced by 0.2dB/mm from room temperature of 24^0C to 105^0C. For the 50% mixture the losses have gone down by 0.15dB/mm from room temperature of 27^0Cto 84^0C. So heat reduces the loss of the liquids except for FC40. For FC40 the transmission loss remains fairly constant at 3 GHz. The loss free analysis for the extraction of the dielectric constant fails after 3 GHz for all the liquids except FC40. Ethylene glycol has fewer variations in dielectric constant within 3 GHz relative to DI H_2O & 50% mixture solution. The dielectric constant extracted using the algorithm for the 50% mixture is in between the DI H_2O and the ethylene glycol.

CHAPTER 4
ANALYSIS OF BANDSTOP FILTER WITH RESONANT CIRCUIT TUNING CAPABILITY USING RF FLUIDS

4.1 Introduction

This chapter investigates the use of fluids as a tuning mechanism in a microstrip and coplanar waveguide stub circuit. There are many ways to tune bandstop filters for example in [33], thermal actuators and square plates are used as tuning elements to change the loading effect of slot resonators etched in the ground plane. In [34] a piezoelectric transducer with an attached dielectric perturber is used to tune the bandstop filter. Liquid metal in a Teflon solution is utilized in a coplanar waveguide line to behave as a switch [35]. Liquids used as a superstrate to tune passive structures is seen in [5], [36]. This work studies the impact of lossy deionized water (DI H_2O) placement on planar tuning designs. The fluid offers the potential advantage of high dielectric constant (ε_r = 78 at 3 GHz) [22] which can significantly extend tuning range. However, it also offers the challenge of high loss (tan delta=0.54 at 10 GHz) which reduces signal strength. The focus of the study investigates the tuning range capability based on placement in microwave resonator stub design that behaves like a bandstop filter and to determine which offers better performance.

4.2 Design Approach

Each stub design (coplanar waveguide and microstrip) is designed to resonate at 2.14 GHz and is built on FR4 (ε_r = 4.78 and tan delta=0.02) with copper thickness of 1.4 mils. The fluid is housed in channels made from PDMS (PolyDimethylSiloxane)[37] secured on top of the FR4 board. The fluid channels are 2 mm wide, 15 mm long and 2 mm tall. At the end of the stub, the channel is 4mm wide. The channel locations are placed at maximum electric field positions for the different resonance frequencies along the stub

length based on odd multiples of λ/4 resonances. In this work, the positions are based in the +y direction in Fig. 4.1(a, b). For example the electric field for the first resonance (λ/4) is maximum at the end of the stub(y=0). If lstub is the length of the stub, the second resonance (3λ/4) has maximum Electric field at y=0, 2*lstub/3. The third resonance (5λ/4) has maximum Electric field at y=0, 2*lstub/5 and 4*lstub/5. Therefore the maximum electric field associated with mλ/4 resonance, where m is odd can be determined by y_{mn}= n*lstub/m, where m is the order of resonance and n is the half wavelength order.

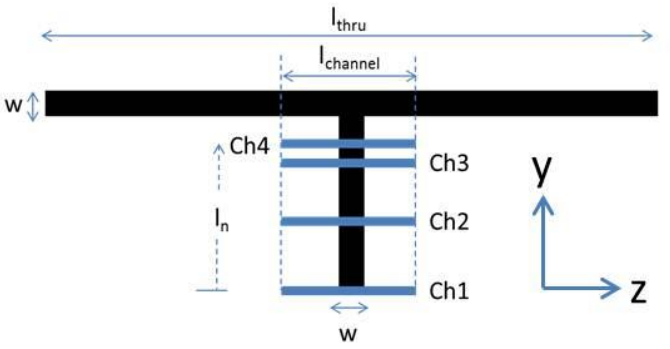

a) Microstrip layout

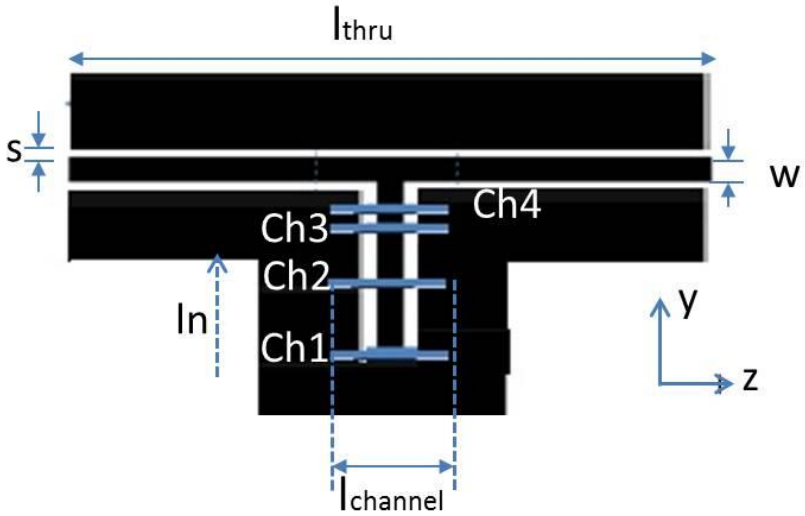

(b) Coplanar Waveguide layout

Figure 4.1 (a) Layout of microstrip resonator stub and (b) Layout of coplanar waveguide resonator stub with fluidic channels indicated in blue

The designs have a similar layout and are described in the following notation – microstrip (coplanar). The substrate thickness is 60 mils (30 mils). The coplanar waveguide excites higher order modes for 60 mils, therefore the substrate thickness is chosen to be 30 mils. The stub length is 18 (19.737) mm. The channel centers are placed at (a) 7.2 (7.9) mm, (b) 12 (13.2) mm, (c) 14.4(15.8) mm relative to the end of the stub. The reference positions in the circuit dimensions are zero-width lines for ease of reading. The measured dimensions of the microstrip and coplanar waveguide structure is listed in Table 4.1 and 4.2 respectively.

Table 4.1:- Dimensions of the microstrip stub structure depicted in Fig 4.1(a) and the locations of the channels

W	2.762 mm
l1	7.2 mm
l2	12 mm
l3	14.4 mm
l_{stub}	18 mm
l_{thru}	65 mm

Table 4.2:- Dimensions of the coplanar waveguide stub structure depicted in Fig 4.1(b) and the locations of the channels

W	1 mm
S	0.48 mm
Wg	7 mm
l1	7.9 mm
l2	13.2 mm
l3	15.8 mm
l_{stub}	19.737 mm
l_{thru}	71.3 mm

The designs are modelled and simulated using Ansys HFSS [38] and Q3D [39]. For DI H_2O the Multipole Debye model is utilized to factor in the frequency dependence of dielectric constant and loss tangent. The values of these properties at different frequencies is well researched in the literature [22], [23]. The measurement results are obtained on the Anritsu 37369D Network Analyzer for the frequency 0.1 GHz to 14GHz. A full two-port calibration is used to establish the reference planes at the SMA connector interface to the board.

4.3 Fabrication

The structure in Fig. 4.1(a) and (b) is fabricated using the C60 LPKF Milling Machine. FR4 is used as the substrate. The fluid housing channels are created using PDMS (Poly Dimethyl Siloxane). First a glass mold is designed to create the desired channel shape. 10:1 mixture of PDMS (Dow Corning Sylgard 184) [37] and (silicone: hardener) is poured onto the mold. This is allowed to solidify by heating it to 70^0C for 4 hrs. The hardened PDMS is removed from the mold and adhered to the substrate with the PDMS adhesive (Dow Corning SE 9187L) [40]. The PDMS fabrication procedure is discussed in detail in Appendix E. The DI H_2O is mixed with a color dye for ease of visibility. SMA connector is soldered to the edge of the board.

4.4 Microstrip Stub Results

The fabricated circuit, shown in Fig. 4.2, has four fluid channels similar to those in Fig. 4.1(a). In the following discussion, the resonance orders are related to case numbers where the 1st resonance ($\lambda/4$) is case 2-channel 1 filled, 2^{nd} resonance ($3\lambda/4$) is case 3-channel 1&3 filled and 3^{rd} resonance ($5\lambda/4$) is case 4-channel 1,2 & 4 filled. A summary is shown in Table 4.3.

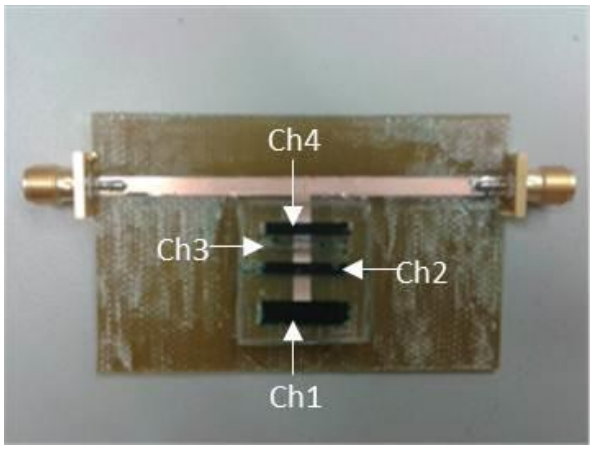

Figure 4.2 Microstrip design with channels. Dark regions have dyed DI H_2O. Here Channel 3 is empty and channel 1,2 and 4 are filled with DI H_2O (Case 4 in Table 4.3).

Table 4.3. Resonance cases with the corresponding filled channel setup

Case No (resonance)	Liquid Channels
1 (air)	None
2(λ/4)	1
3(3λ /4)	1,3
4(5λ/4)	1,2,4

The reference design for this work is the conventional microstrip with air in the channels. The 1st, 2nd and 3rd resonances of the conventional microstrip are 2.2, 6.4, and 10.5 GHz, respectively. These results are obtained from the simulation and measurement results shown in Fig. 4.3. The effect of the fluid, when added to the different channels based on resonance, is described in Fig. 4.3 for microstrip line.

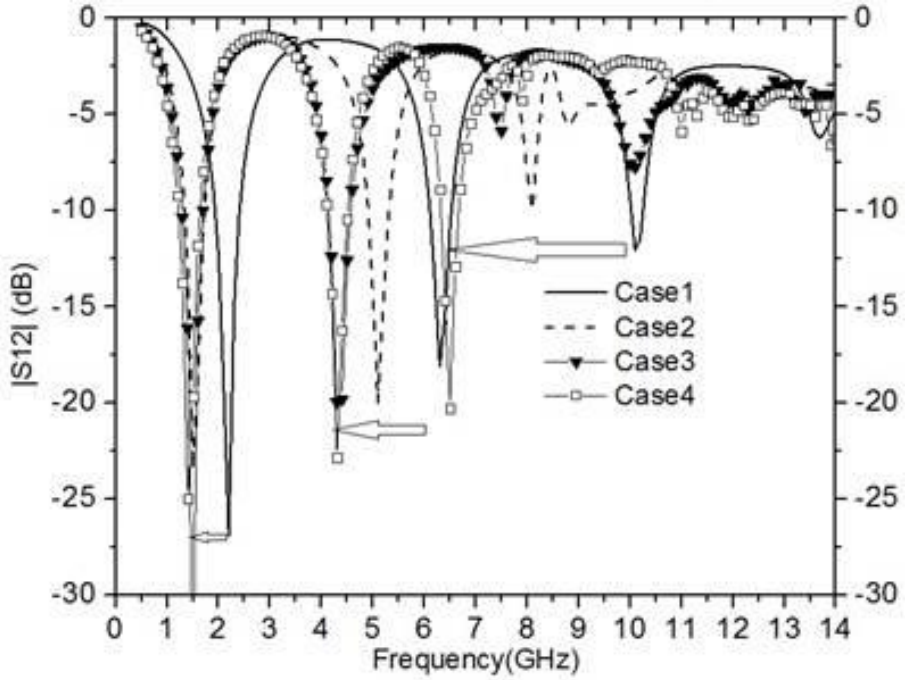

(a) Simulated Microstrip Stub Transmission Data

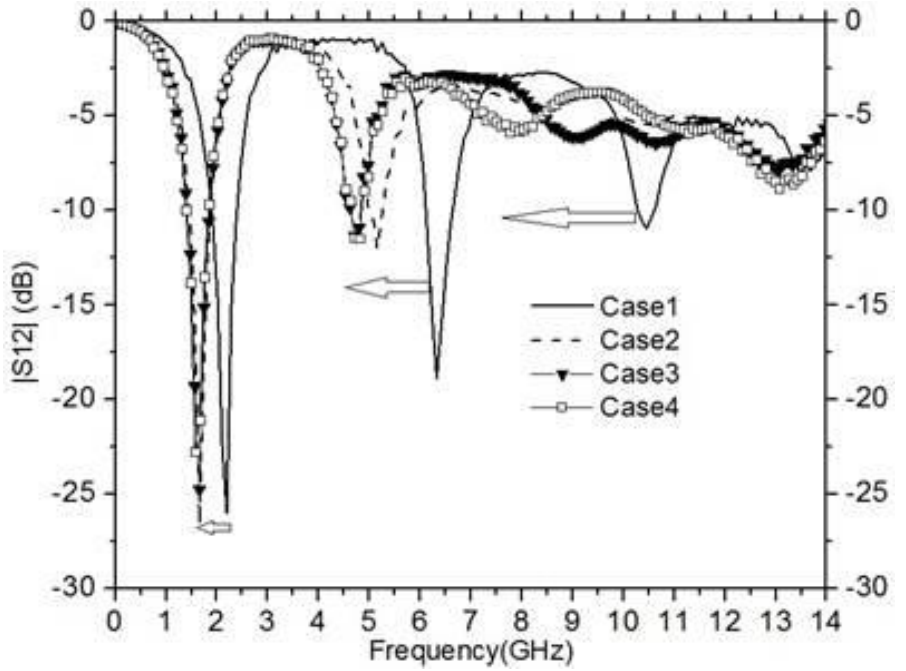

(b)Measurement Microstrip Stub Transmission Data

Figure 4.3 (a) Simulated data and (b) Measurement data for the microstrip fluidic tuning circuit. Case 1,2,3 and 4 correspond to specific channels being filled as listed in Table 4.3.

In Fig. 4.3, when DI H_2O is added to Ch 1 (Case 2) all resonant frequencies shift to a lower frequency. The corresponding shifts relative to the conventional design (Case1) are 1.5 GHz for the first resonance, 5.2 GHz for the second resonance and 9.0 GHz for the third resonance. When the fluid is added to Ch 1 and 3 (Case 3), the first resonance remains the same at 1.5 GHz, and second and third shift to 4.8 GHz and 9.0 GHz respectively. These results are consistent with the simulation data shown in Fig. 4.3(a). Given the high attenuation of DI H_2O, the third resonance degrades considerably. See Table 4.4 for a summary of the measured resonant frequency and insertion loss values for the various microstrip cases.

Table 4.4. Measurement Results at resonance points/nulls in the transmission data for microstrip line

Resonance #	Case 1(GHz, dB)	Case 2(GHz, dB)	Case 3(GHz, dB)	Case 4(GHz, dB)
1	2.2, -26	1.5, -27	1.5 -25	1.4, -23
2	6.4, -19	5.2, -11.5	4.8, -11	4.8, -11
3	10.5, -11	9.0, -6	9.0, -6	7.8, -6

4.5 Coplanar Waveguide Stub Results

The simulated results for the coplanar waveguide structure is shown in Fig. 4.4, has channel placement theory/design as described previously in Section 4.2. As seen in Fig. 4.3 and 4.4 the resonant frequencies of the reference structures (no channels filled-Case 1) for coplanar waveguide and microstrip line are identical. When DI H_2O is added to Ch1, all resonant frequencies shift by 0.3 GHz lower than the same microstrip design case. When the fluid is added to Ch1 and Ch3 (Case 3) the first resonance remains the same at 1.1 GHz, and second and third shift to 2.9 GHz and 6.9 GHz, lower than that seen in microstrip.

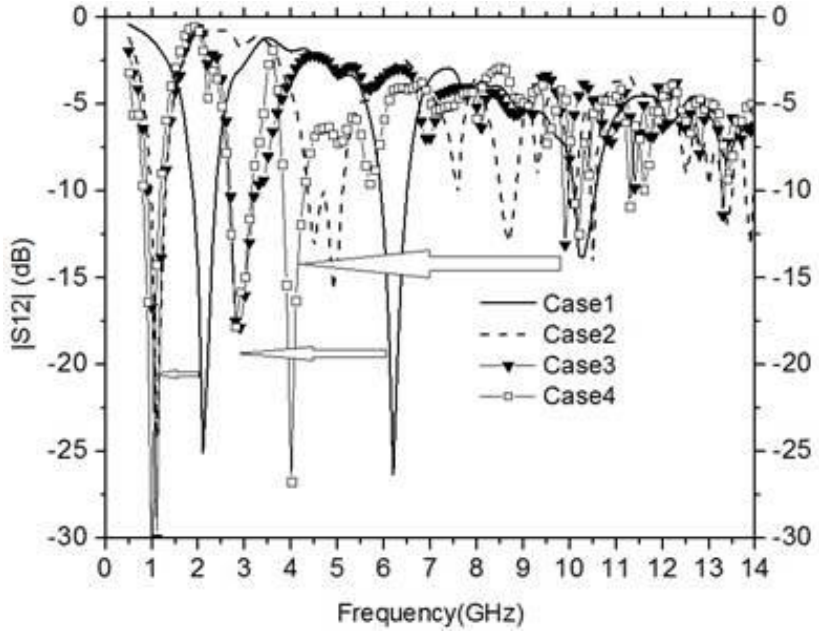

Figure 4.4 Simulated data for the fluidic tuning circuit in coplanar waveguide with DI-H_2O.

The coplanar waveguide shows a larger change in frequency shift compared to microstrip due to the higher surface interations with the fluid compared to the fringing fields of the microstrip. A trade-off is that the high losses of the DI H_2O increase the attenuation and noise in the insertion response.

To understand the impact of DI H_2O on circuit parameter values, Q3D was used to analyze changes in impedance capacitance and conductance in the 2D cross-section of each design. For microstrip the changes are: (a) ΔZ=20 ohms, (b) ΔC=234 pF and (c) ΔG=140 mS. For coplanar waveguide the changes are: (a) ΔZ=35 ohms, (b) ΔC=1100 pF and (c) ΔG=3 mS. Thus, coplanar waveguide provides the larger frequency shift as a tuning technique; however, microstrip provides the better attenuation management. But the physical manufacture is difficult.

The liquid containment in a coplanar waveguide was not possible because of the spacing (gap) that runs between the trace and the ground plane along the stub. When liquid is injected into one of the channels, due to the pressure, it flows into the other channel. The gap on either side of the trace acts like a trench between channels, hence making containment of liquid in the channel difficult. The measured results are not accurate, with the technique used in this work for fluid containment. But, if fluid containment is possible, the coplanar waveguide would show better performance as shown in simulation results.

4.6 Conclusions

This chapter investigates the use of fluids as a tuning method for planar circuit technology. The tuning capability in the microstrip and coplanar design offers the ability to achieve discrete tuning based on specific channel selection. This study confirms the feasibility of the design and the realization of a bandstop filter. The coplanar waveguide structure offers higher resonance frequency shifts but at the cost of noise and loss. A tradeoff is made between resonance shifting and loss. A more robust and accurate method of fluid containment is required for the coplanar waveguide.

CHAPTER 5
IMPLEMENTATION OF A PATCH ANTENNA SWITCH USING FLUIDIC STUBS

5.1 Introduction

Reconfigurable passive structures using a liquid metal alloy has been studied in the past [41-43]. The antennas and the filters used in the referenced papers use eutectic gallium indium (EGaIn) to tune the frequency of resonance by changing the shape of the structure. Non-metal liquids have been used in reconfigurable design structures to tune antennas/filters and phase shifters [5-7]. In all of the above work the liquid has been directly utilized on the operational structure (antenna, FSS and phase shifter) with the loss of the structure dependent on the dielectric loss of the liquid. This chapter presented here uses the liquids on a stub that is not connected to the direct signal path as seen in Fig. 5.1, thereby ensuring that the dielectric loss of the liquid does not affect the overall propagation loss of the system. The antenna is designed to radiate at 5 GHz and the length of the open shunt stub is $\lambda/4$ at 5GHz, thereby forming a short to ground. The liquid channel at the end of the stub converts the open to a short at 5 GHz. Deionized water (DI H_2O) with its high dielectric constant (ε_r=73.75) provides high tuning capability.

5.2 Design Approach

The microstrip patch antenna is designed to radiate at 5GHz using equations from literature [44]. A layout is shown in Fig. 5.1 of the microstrip circuit with microfluidic channel. The length of the open shunt stub is $\lambda/4$ at 5GHz, which transfers to a short to ground at the junction of the feedline and the stub. This ensures that no signal goes to the antenna and hence does not radiate when the liquid channel is empty (air). When the

channel is filled with DI H_2O the stub does not look like a short at the junction but converts to an open. This allows the signal to reach the antenna and hence radiate at the design frequency.

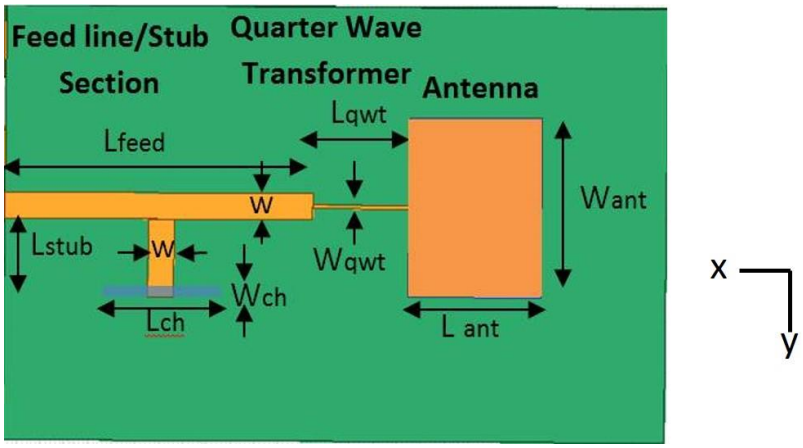

Figure 5.1. Patch Antenna Schematic with feed, stub and quater wave transformer

The patch antenna was designed using Ansys HFSS [38]. First the patch antenna with a feedline is simulated to find the impedance at the edge of the antenna. By de-embedding the feedline (shifting reference plane), the input impedance at the edge of the antenna is 260.1Ω. Using the reference impedance as 50 Ω the Quarter Wave Transformer impedance is calculated to be 114.2 Ω. The feedline is λ long at the design frequency of 5 GHz. The final lengths are calculated by compensating the open end effects at the junctions. The Hammerstad equations are used to calculate the open end effect lengths [45,46]. The open end effect at the feedline-transformer and the transformer-antenna junction is 0.545mm and 0.64mm respectively. The dimensions of the structure depicted in Fig. 5.1 are listed in Table 5.1.

Table 5.1:- Dimensions of the structure depicted in Fig. 5.1	
Want	17.65 mm
Wqwt	0.35 mm
W	2.58 mm
Wch	2.0 mm
Lant	13.29 mm
Lqwt	9.87 mm
Lch	15 mm
Lfeed	30.97 mm
Lstub	7.7 mm

For DI H_2O the Multipole Debye model is utilized to factor in the frequency dependence of dielectric constant and loss tangent. The values of these properties at different frequencies is well researched in the literature [22] and [23].

5.3 Fabrication

The structure in Fig. 5.1 is fabricated using the C60 LPKF Milling Machine. FR4 is used as the substrate. The dielectric constant and loss tangent of FR4 is 4.2 and 0.015 respectively at 5 GHz. The thickness of the copper is 1.4mils. The fluid housing channels are created using PDMS (Poly Dimethyl Siloxane). First a glass mold is designed to create the desired channel shape. 10:1 mixture of PDMS (Dow Corning Sylgard 184) [37] and (silicone: hardener) is poured onto the mold. This is allowed to solidify by heating it to 700C for 4 hrs. The hardened PDMS is removed from the mold and adhered to the substrate with the PDMS adhesive (Dow Corning SE 9187L) [40]. The PDMS fabrication procedure is discussed in detail in Appendix E. The DI H_2O is mixed with a color dye for ease of visibility. SMA connector is soldered to the edge of the board. The fabricated design is seen in Fig 5.2

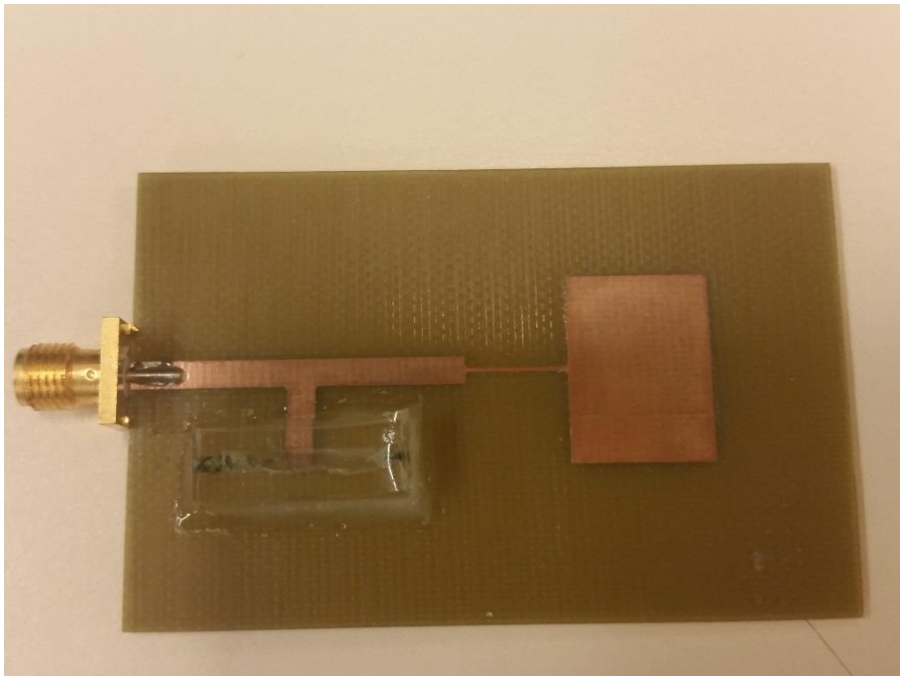

Figure 5.2. Fabricated patch antenna structure with feedline, stub, pdms channel with no liquid and quarter wave transformer.

5.4 Results

The stub is modeled in Ansys HFSS [38] to extract the impedance it produced at the junction to the feedline. The shunt stub appears as a parallel circuit element in Fig. 5.3. When the fluid channel is empty the Zstub = 19.94 Ω. This values is as expected, as the open circuit at the open end transfers to a short circuit at λ/4 at the junction, hence the low value. When DI H_2O is added in the channel the Zstub = 121.31 Ω. This change occurs because the open circuit at the open end with the fluid is transformed into a short circuit, this short circuit then is transferred to an open circuit at λ/4 at the junction.

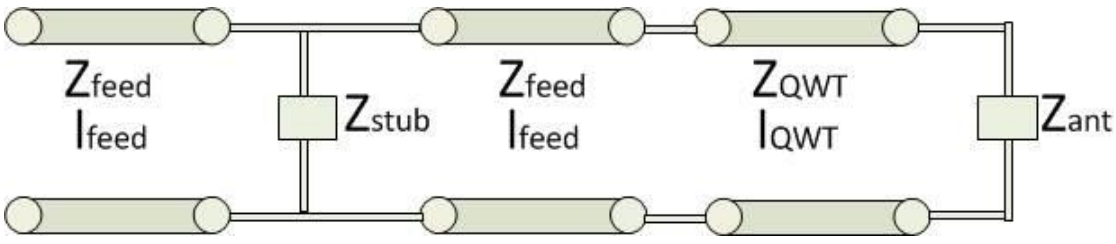

Figure 5.3. Distributed transmission line equivalent –circuit model of Fig. 5.1

The simulated and measured results of the return loss (S11) is shown in Fig. 5.4. The simulation is in close agreement to the measured data. The switching behavior is seen in the highlighted region at around 5 GHz. The OFF S11 value is -1dB and the ON S11 value is -12dB. The antenna indicates that at 5 GHz the antenna radiates whereas the black curve at 5GHz shows that the stub prevents the antenna from radiating.

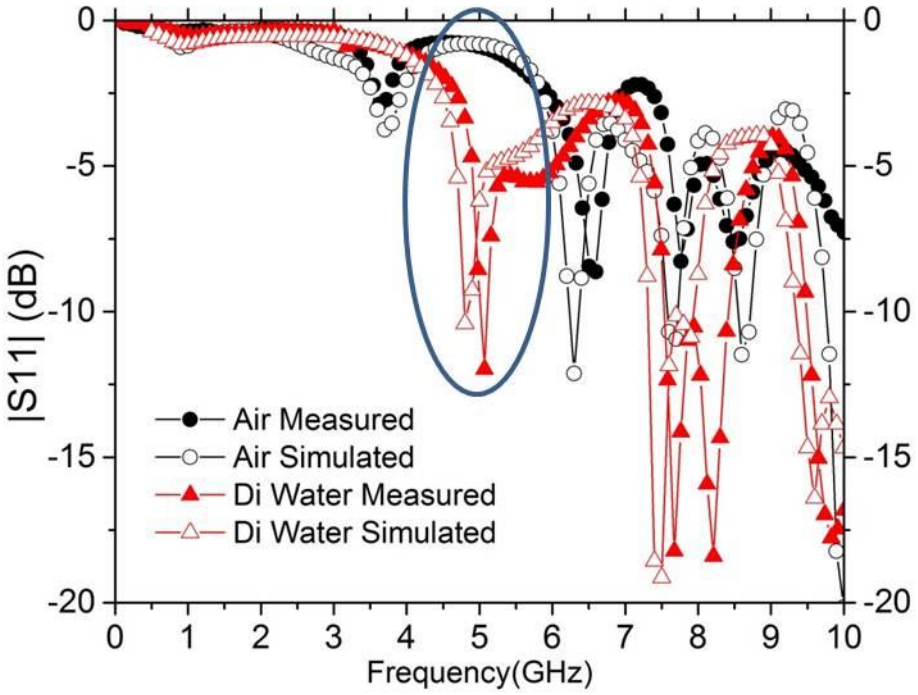

Figure 5.4. Measured and simulated magnitude of S11 results for air and DI H_2O.

As mentioned earlier the addition of DI H_2O (high loss) does not degrade the S11. This is a result of the liquid channel being away from the direct path of the signal to the antenna. The measured radiation pattern of the patch antenna with and without DI H_2O is shown in Fig. 5.5. The red curve for both the E and H plane is approximately 10 dB below the purple curve. This shows that the antenna structure with DI H_2O radiates while the

structure without DI H_2O does not radiate. The antenna measurement is taken in a chamber with 0 dB as the power input into the antenna.

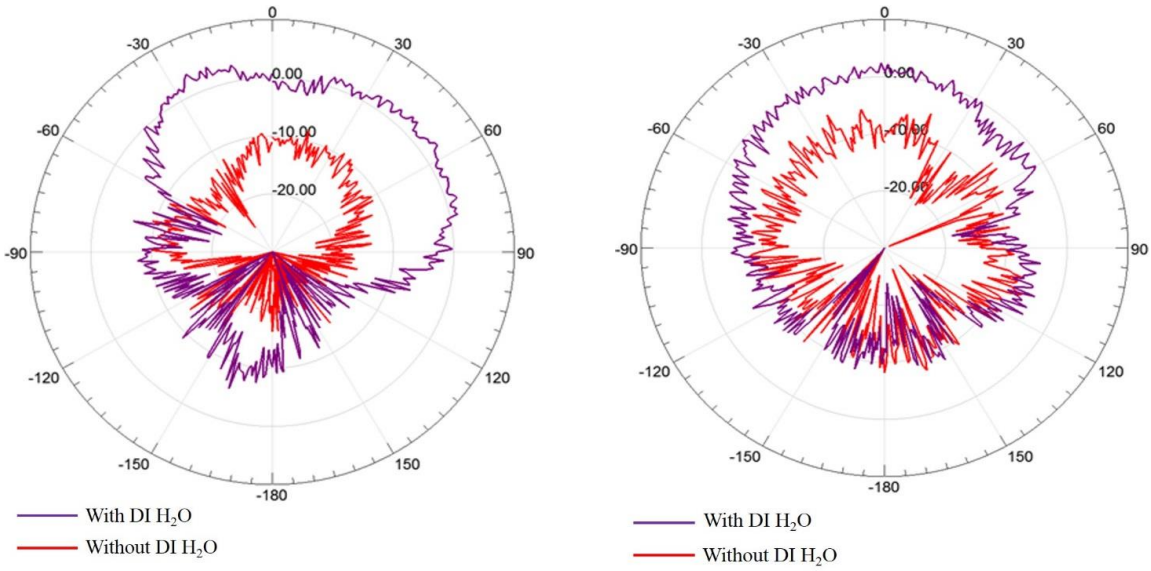

(a) E Plane (xz) (b) H Plane (yz)

Figure 5.5. Measured Radiation Pattern of the Antenna. Purple curve depicts the radiation pattern of the antenna structure with DI H_2O and the red curve depicts the radiation pattern of the antenna structure without DI H_2O .

The xz-E plane measured pattern in Fig. 5.5 (a) is distorted and deviates from the patch antenna pattern. This is attributed mainly due to the feedline and the stub interfering in the radiation. The yz-H plane pattern has a small notch at 80 degrees, this can be attributed to the antenna chamber measurement setup error. The simulated radiation pattern of the patch antenna with DI H_2O is shown in Fig. 5.6. The problem with the feedline and the stub interfering in the radiation is also captured in the simulated result at the E(xz) plane curve (dotted red).

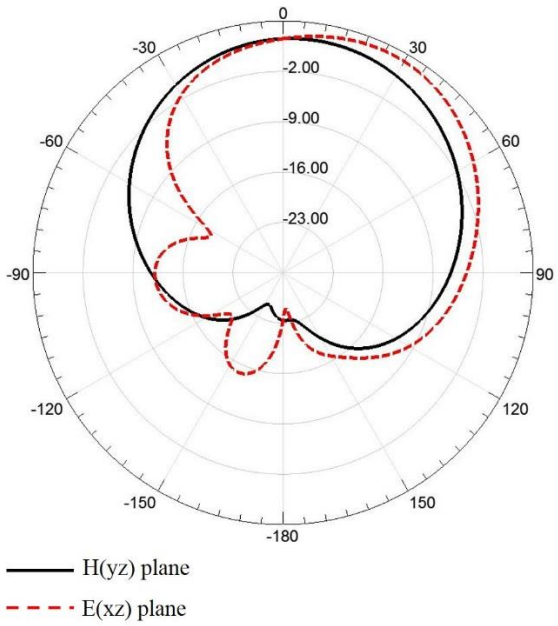

Figure 5.6. Simulated radiation pattern of the antenna with DI H_2O. black curve depicts the pattern along the H (yz) plane and the red curve depicts the pattern along the E (xz) plane

Table 5.2 shows the peak directivity, peak gain, radiation efficiency and peak realized gain at 5 GHz. The values clearly show that the air case does not radiate while the DI H_2O radiates. The distortion in the pattern does not affect the beam area of the antenna. The beam area in the E and the H plane is 2.77.

Table 5.2:- Simulated Antenna Radiation Parameters for the 2 cases- Air and DI H_2O

	Peak Directivity (dB)	Peak Gain(dB)	Radiation Efficieny (dB)	Peak Realized Gain (dB)
Air	4.07	-2.19	-6.26	-9.83
DI H_2O	5.54	3.4	-2.139	3.09

The amount of distortion and the peak radiation power increases with the length of the feedline. A simulation study was conducted to capture the effect of the feedline on the radiation pattern of the patch antenna. In this study the feedline is varied as λ, $\lambda/2$ and $\lambda/6$ and its radiation pattern in the E (xz) plane is seen in Fig. 5.7(a). This structure is made

up of the feedline, QWT and the patch. For this simulation study the stub and the fluid channels are removed. We see that as the feedline decreases the pattern gets more symmetric. As the feedline increases to λ the distortion in the E plane increases. The H plane radiation is not shown as it is not affected by the change in length of the feedline. Since the above simulation does not take into effect the open stub radiation, another study to capture the effect of change in feedline length with the stub and the DI H_2O is undertaken. Fig. 5.7 (b) shows the E plane radiation pattern for feedline length=λ and λ/2.

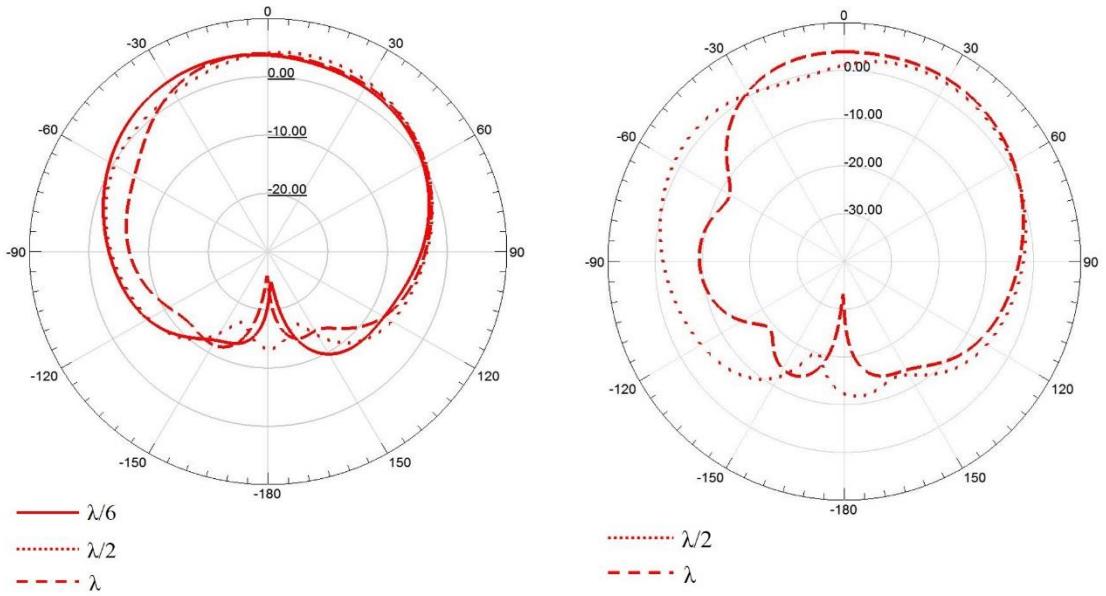

(a) (b)

Figure 5.7.(a) Simulated radiation pattern in the E(xz) plane of the variable feed length antenna without the stub and DI H_2O. (b) Simulated radiation pattern in the E(xz) plane of the variable feed length antenna with the stub and DI H_2O

As seen in Fig. 5.7(b). With the addition of stub and DI H_2O the distortion increases. The radiation pattern of the original structure given in Fig. 5.1 is a combination of the radiation produced by the feedline, stub and QWT along with that of the patch antenna. The

H plane radiation is not shown as it is not affected by the change in length of the feedline. The 3dB beamwidth is not affected by this distortion and hence will not pose a great problem in the functioning of this antenna setup.

5.5 Conclusions

It has been shown that the fluidic stub used herein can act as a switch in an antenna configuration. The OFF/ON S11 values are -1dB and -12dB respectively. There is a distortion in the radiation pattern in the E plane which has been attributed to the radiation contribution from the feedline and the open stub. Since the radiation in the 3dB beamwidth of the main lobe is intact this patch antenna configuration proves to be a good working model. This prototype can be used as a liquid sensor in machines that use liquids for cooling. The ON/OFF functioning can signal a leakage in the system.

CHAPTER 6

CONCLUSION AND FUTURE WORK

6.1 Summary and Conclusions

In chapter 2, a microstrip test structure and an extraction algorithm was designed to extract the dielectric properties of a liquid. In Chapter 3, a coplanar waveguide structure was fabricated as an alternate and more efficient structure than that discussed in Chapter 2. Analysis of change in dielectric properties of different fluids with heat using the coplanar waveguide structure was undertaken. Based on the study done in Chapter 2 and Chapter 3, DI H_2O is used as a tuning liquid in Chapter 4 and Chapter 5. Chapter 4 shows the resonant circuit tuning that can be achieved with DI H_2O. By placing the liquid strategically at localized positions along the stub, a combination of tunable ranges at different center frequencies is achieved. Chapter 5 shows the switching characteristic property that can be achieved using a DI H_2O stub in a patch antenna configuration. DI H_2O has excellent tuning capability due to its high dielectric constant, but its dielectric properties change with heat considerably as seen in Chapter 3. FC40 and other low loss liquids which have low dielectric constant have stable, constant dielectric properties that do not change with temperature.

6.2 Future Work

This work shows the potential use that liquids can have in RF circuits. However, an ideal liquid to be used in RF circuits would be one that has high dielectric constant and does not show variation in its dielectric properties due to heat. An extraction algorithm to extract the dielectric properties, which incorporates loss into the calculations needs to be developed. This would give an accurate value for dielectric constant. Also an automated fluid injection system will be needed to maintain a known constant fluid speed, which will yield predictable/repeatable results.

This automated fluid injection system can also then be used to obtain transient characteristics of the liquid switch. Finally, additional studies are needed to identify a more efficient method to fabricate channels and housing to contain the liquids used on different substrates..

Bibliography

[1] J. Li and H. Miyashita, “Post placement thermal via planning for 3D integrated circuit,” *IEEE Asia Pacific Conference on Circuits and Systems*, pp. 808-811, December 2006.

[2] D.A. Benson et. Al, “Micromachined heat pipes in silicon MCM substrates,” *IEEE Multi Chip Module Conference Proceedings*, pp. 127-129, February 1996.

[3] S.V. Garimella et al., “On-chip thermal management with microchannel heat sinks and integrated micropumps,” *Proceedings of the IEEE*, Vol. 94, No. 8, pp. 1534-1548, August 2006.

[4] Chlieh, O.L.; Morcillo, C.AD.; Pavlidis, S.; Khan, W.T.; Papapolymerou, J., "Integrated microfluidic cooling for GaN devices on multilayer organic LCP substrate," *Microwave Symposium Digest (IMS), 2013 IEEE MTT-S International* , vol., no., pp.1,4, 2-7 June 2013.

[5] Murray, C.; Franklin, R.R., "Frequency tunable fluidic annular slot antenna," *Antennas and Propagation Society International Symposium (APSURSI), 2013 IEEE* , vol., no., pp.386,387,7-13July2013.

[6] Kelley, M.S.; Huff, G.H., "Fluidic tuning of a frequency selective surface based on a four-arm Archimedean spiral," *Antennas and Propagation Society International Symposium,APSURSI),2013IEEE*,vol.,no.,pp.468,469,7-13,July-2013.

[7] Meineri, P.; Dubuc, D.; Grenier, K., "Liquid-based tunable loaded-line phase shifter," *Microwave Conference (EuMC), 2012 42nd European* , vol., no., pp.719,722, Oct. 29 2012-Nov. 1 2012.

[8] Huff, G.H.; Rolando, D.L.; Walters, P.; McDonald, J., "A Frequency Reconfigurable Dielectric Resonator Antenna Using Colloidal Dispersions," *Antennas and Wireless Propagation Letters, IEEE* , vol.9, no., pp.288,290, 2010.

[9] Murray, Casey, and Rhonda R. Franklin. "EDGE coupled variable microfluidic directional coupler." *Microwave and Optical Technology Letters* 55.4 (2013): 756-758.

[10] Meissner, T.; Wentz, F.J., "The complex dielectric constant of pure and sea water from microwave satellite observations," *Geoscience and Remote Sensing, IEEE Transactions on* , vol.42, no.9, pp.1836,1849, Sept. 2004.

[11] ME Global Ethylene Glycol, http://www.meglobal.biz/media/product_guides/MEGlobal_MEG.pdf .

[12] 3M Flourinert Electronic Liquid FC40, http://multimedia.3m.com/mws/mediawebserver?mwsId=66666UgxGCuNyXTtnxTEo8s6EVtQEcuZgVs6EVs6E666666--&fn=prodinfo_FC40.pdf.

[13] Booth, J.C.; Mateu, J.; Janezic, M.; Baker-Jarvis, J.; Beall, J-A, "Broadband Permittivity Measurements of Liquid and Biological Samples using Microfluidic Channels," *Microwave Symposium Digest, 2006. IEEE MTT-S International* , vol., no., pp.1750,1753, 11-16 June 2006.

[14] MOUKANDA, M., et al. "COMPLEX PERMITTIVITY EXTRACTION USING TWO TRANSMISSION LINE S-PARAMETER MEASUREMENTS." *The African Review of Physics* 2.3 (2009).

[15] Suster, M.A; Mohseni, P., "An RF/microwave microfluidic sensor based on a center-gapped microstrip line for miniaturized dielectric spectroscopy," *Microwave Symposium Digest (IMS), 2013 IEEE MTT-S International* , vol., no., pp.1,3, 2-7 June 2013.

[16] Garcia-Banos, B.; Canos, AJ.; Catala-Civera, J.M.; Plaza-Gonzalez, P.J., "Accurate permittivity measurements with a coaxial resonator independently of coupling level," *Microwave Symposium Digest (IMS), 2013 IEEE MTT-S International* , vol., no., pp.1,3, 2-7 June 2013.

[17] Helmy, AA; Kabiri, S.; Bajestan, M.M.; Entesari, K., "A miniaturized spectroscopy system for complex permittivity detection of organic mixtures in the 0.65–2 GHz frequency range," *Microwave Symposium Digest (IMS), 2013 IEEE MTT-S International* , vol., no., pp.1,4, 2-7 June 2013.

[18] Valvoline Zerex G-05 Antifreeze/Coolant, http://www.valvoline.com/pdf/Zerex_G-05_AFC_Technical_Bulletin.pdf

[19] D.M. Pozar, *Microwave Engineering*, 3rd Ed., John Wiley & Sons, Inc., 2005.

[20] Agilent EEs of EDA, *Advanced Design System (ADS)*, Version 2011.01, Keysight Technologies, Englewood, CO, 2013.

[21] Milling Machine PhotoMat C60, LPKF, Inc. Wilsonville, OR, 1976.

[22] Kaatze, Udo. "Complex permittivity of water as a function of frequency and temperature." *Journal of Chemical and Engineering Data* 34, no. 4 (1989): 371-374.

[23] Zahn, Markus, Yoshimichi Ohki, David B. Fenneman, Ronald J. Gripshover, and V. H. Gehman Jr. "Dielectric properties of water and water/ethylene glycol mixtures for use in pulsed power system design." *Proceedings of the IEEE* 74, no. 9 (1986): 1182-1221.

[24] Booth, J.C.; Orloff, N.D.; Mateu, J.; Janezic, M.; Rinehart, M.; Beall, J-A, "Quantitative Permittivity Measurements of Nanoliter Liquid Volumes in Microfluidic Channels to 40 GHz," *Instrumentation and Measurement, IEEE Transactions on* , vol.59, no.12, pp.3279,3288, Dec. 2010.

[25] Raj, A; Holmes, W.S.; Judah, S.R., "Wide bandwidth measurement of complex permittivity of liquids using coplanar lines," *Instrumentation and Measurement, IEEE Transactions on* , vol.50, no.4, pp.905,909, Aug 2001.

[26] Sanghyun Seo,; Stintzing, Thomas; Block, Ian; Pavlidis, D.; Rieke, Matthias; Layer, Paul G., "High frequency wideband permittivity measurements of biological substances using coplanar waveguides and application to cell suspensions," *Microwave Symposium Digest, 2008 IEEE MTT-S International* , vol., no., pp.915,918, 15-20 June 2008.

[27] Ru-Yuan Yang; Su, Yan-Kuin; Min-Hang Weng; Cheng-Yuan Hung; Hung-Wei Wu, "Characteristics of coplanar waveguide on lithium niobate crystals as a microwave substrate," *Journal of Applied Physics* , vol.101, no.1, pp.014101,014101-5, Jan 2007

[28] Surducan, E., V. Surducan, and C. Neamtu. "Measurements of the liquids dielectric properties changes with temperature for microwaves power processing optimization." *PROCESSES IN ISOTOPES AND MOLECULES (PIM 2011)*. Vol. 1425. No. 1. AIP Publishing, 2012.

[29] Gupta, Kuldip C., Ramesh Garg, and Inder J. Bahl. "Microstrip lines and slotlines." (1979).

[30] Wen, Cheng P. "Coplanar waveguide: A surface strip transmission line suitable for nonreciprocal gyromagnetic device applications." *Microwave Theory and Techniques, IEEE Transactions on* 17.12 (1969): 1087-1090.

[31] Ghione, Giovanni, and Carlo U. Naldi. "Coplanar waveguides for MMIC applications: Effect of upper shielding, conductor backing, finite-extent ground planes, and line-to-line coupling." *Microwave Theory and Techniques, IEEE Transactions on* 35.3 (1987): 260-267.

[32] Ghione, Giovanni, and C. Naldi. "Analytical formulas for coplanar lines in hybrid and monolithic MICs." *Electronics Letters* 20.4 (1984): 179-181.

[33] Yan, W.D.; Mansour, R.R., "Compact Tunable Bandstop Filter Integrated with Large Deflected Actuators," *Microwave Symposium, 2007. IEEE/MTT-S International* , vol., no., pp.1611,1614, 3-8 June 2007.

[34] Lung-Hwa Hsieh; Kai Chang, "Piezoelectric transducer tuned bandstop filter," *Electronics Letters* , vol.38, no.17, pp.970,971, 15 Aug 2002.

[35] Chung-Hao Chen; Whalen, J.; Peroulis, D., "Non-Toxic Liquid-Metal 2-100 GHz MEMS Switch," *Microwave Symposium, 2007. IEEE/MTT-S International* , vol., no., pp.363,366, 3-8 June 2007.

[36] Murray, C.; Franklin, R.R., "Fluidically adjustable degenerate mode microstrip ring filter," *Wireless and Microwave Technology Conference (WAMICON), 2014 IEEE 15th Annual* , vol., no., pp.1,3, 6-6 June 2014.

[37] Dow Corning PDMS, http://www.dowcorning.com/applications/search/products/details.aspx?prod=010 64291, accessed December 2013.

[38] Ansys, *High Frequency Structure Simulator (HFSS)*, Version 15, Ansoft Corporation, Pittsburgh, PA, 2013.

[39] Ansoft, Q3D Extractor, Version 10, Ansoft Corporation, Pittsburgh, PA, 2012.

[40] Dow Corning SE 9187 L, http://www.dowcorning.com/applications/search/products/details.aspx?prod=02511941&type=PROD, accessed December 2013.

[41] Dey, A; Guldiken, R.; Mumcu, G., "Wideband frequency tunable liquid metal monopole antenna," *Antennas and Propagation Society International Symposium (APSURSI), 2013 IEEE* , vol., no., pp.392,393, 7-13 July 2013.

[42] Khan, M.R.; Hayes, G.J.; Zhang, S.; Dickey, M.D.; Lazzi, G., "A Pressure Responsive Fluidic Microstrip Open Stub Resonator Using a Liquid Metal Alloy," *Microwave and Wireless Components Letters, IEEE* , vol.22, no.11, pp.577,579, Nov. 2012

[43] Aïssa, B., et al. "Fluidic patch antenna based on liquid metal alloy/single-wall carbon-nanotubes operating at the S-band frequency." *Applied Physics Letters* 103.6 (2013): 063101.

[44] C. A Balanis, *Antenna Theory:Analysis and Design*, 3rd ed. New York:Wiley, 2005, pp. 816-825.

[45] Hammerstad, E.O., "Equations for Microstrip Circuit Design," *Microwave Conference, 1975. 5th European* , vol., no., pp.268,272, 1-4 Sept. 1975.

[46] Silvester, P., and Peter Benedek. "Equivalent capacitances of microstrip open circuits." *Microwave Theory and Techniques, IEEE Transactions on* 20.8 (1972): 511-516.

APPENDIX A

Microstrip Line Width Flowchart

Flowchart to extract the physical dimensions of the microstrip line.

Z_0 - characteristic impedance

e_len – effective length

d – height of substrate

w – width of microstrip line

εr– dielectric constant of substrate

εf– dielectric constant of surrounding medium(superstrate)

εeff – effective dielectric constant

εr1 – dielectric constant of medium (fluid) and board for ADS usage with $\varepsilon_f = 1$

$$\varepsilon eff = \frac{\varepsilon r + \varepsilon f}{2} + \frac{\varepsilon r - \varepsilon f}{2\sqrt{1 + 12\,(\frac{d}{w})}} \qquad \text{A.1}$$

$$Z_0 = \frac{120\pi}{\sqrt{\varepsilon eff}(\frac{w}{d} + 1.393 + 0.667\ln(\frac{w}{d} + 1.444))} \quad , \quad \frac{w}{d} > 1 \qquad \text{A.2}(a)$$

$$= \frac{60}{\sqrt{\varepsilon eff}}\ln(\frac{8d}{w} + \frac{w}{4d}) \quad , \quad \frac{w}{d} < 1 \qquad \text{A.2(b)}$$

calc - excel file with εeff and Z_0 for d/w as a parameter using equations 1,2.

Step 1

Step 2

Step 3

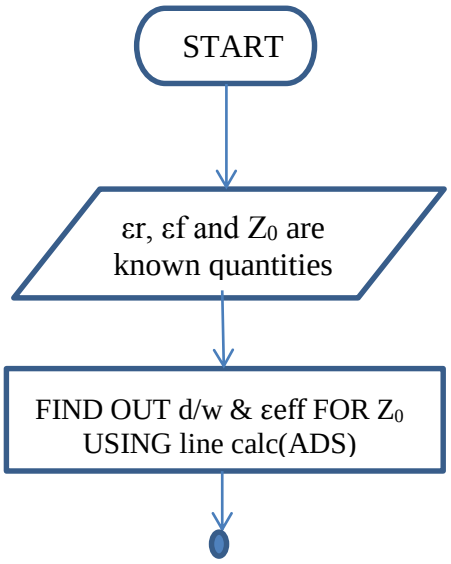

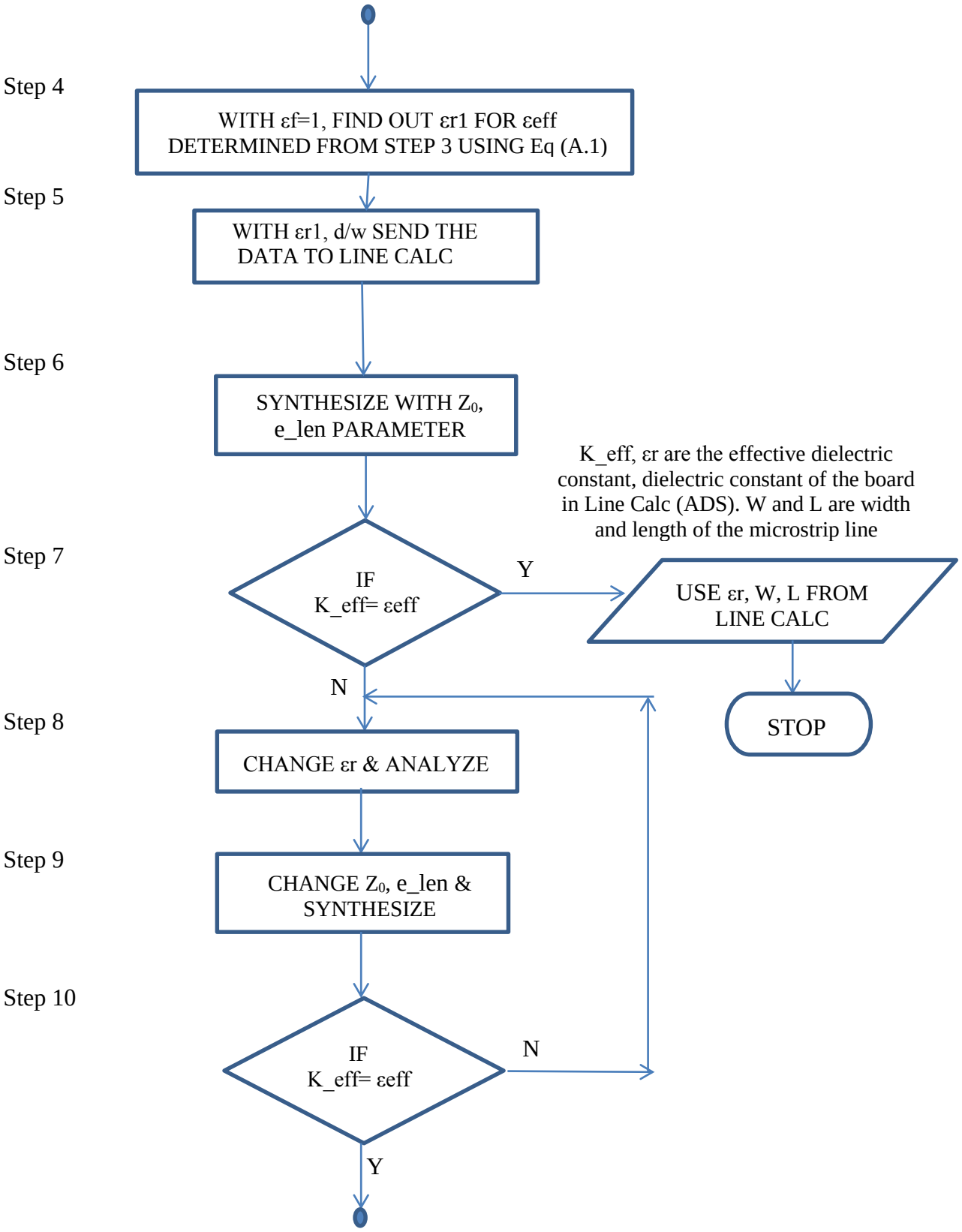
Step 4
WITH εf=1, FIND OUT εr1 FOR εeff DETERMINED FROM STEP 3 USING Eq (A.1)
Step 5
WITH εr1, d/w SEND THE DATA TO LINE CALC
Step 6
SYNTHESIZE WITH Z0, e_len PARAMETER
K_eff, εr are the effective dielectric constant, dielectric constant of the board in Line Calc (ADS). W and L are width and length of the microstrip line
Step 7
IF K_eff= εeff
Y
USE εr, W, L FROM LINE CALC
STOP
N
Step 8
CHANGE εr & ANALYZE
Step 9
CHANGE Z0, e_len & SYNTHESIZE
Step 10
IF K_eff= εeff
N
Y

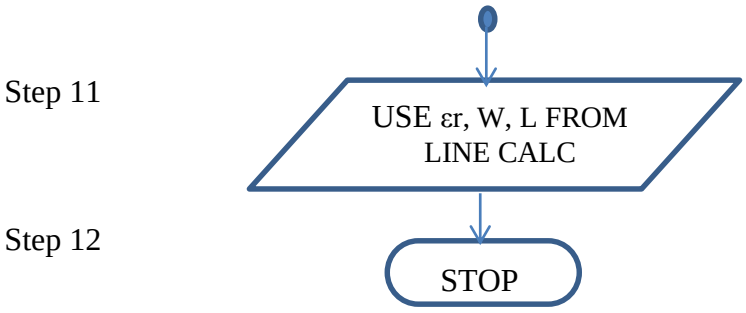

Figure A.1. Flowchart to extract the physical dimensions of the microstrip line for any non-air medium that will reside on top of the conductors in the fluid test cases.

APPENDIX B

Dielectric Extraction Using Microstrip Line

Equation B.1 represents the effective dielectric constant equation and B.2 represents the general equation for extraction of εeff from phase of S21- transmission

$$\varepsilon eff = \frac{\varepsilon r + \varepsilon f}{2} + \frac{\varepsilon r - \varepsilon f}{2\sqrt{1 + 12\,(\frac{d}{w})}} \qquad \text{Eq B. 1}$$

$$\varepsilon eff = (\frac{(\vartheta_{l(rad)} - \vartheta_{s(rad)}) * c}{2\pi f(l_l - l_s)})\text{^}2 \qquad \text{Eq B. 2}$$

d – height of substrate

w – width of microstrip line

εr – dielectric constant of substrate

εf – dielectric constant of surrounding medium (superstrate)

εeff – effective dielectric constant

l_l – length of long microstrip line

l_s – length of short microstrip line

ϑ_l – phase of S21 for the long transmission line

ϑ_s – phase of S21 for the short transmission line

Using equations B.1 and B.2, it is possible to create equations B.3 & B.4 for extraction of the board dielectric constant with the superstrate as air, ε_f is 1.

$$\varepsilon eff\_air = (\frac{3.54 * 10^9 * (\vartheta_{l(rad)} - \vartheta_{s(rad)})}{f})\text{^}2 \qquad \text{Eq B.3}$$

$$\varepsilon r(\text{board}) = \frac{\varepsilon \text{eff\_air} - 0.3125}{0.6875} \quad \text{Eq B.4}$$

For the extraction of the relative permittivity of the superstrate, two cases were considered:

1) When the dielectric constant of board (FR4) was assumed to be constant at 4.78 (wo fd)
2) When the dielectric constant of the board (FR4) was a function of frequency (w fd), which is extracted through the S parameters using Equations B.3 and B.4

Case 1:- Using equations B.1 & B.2, equations B.5 & B.6 have been derived for FR4 relative permittivity to be a constant i.e. ε_r is 4.78.

$$\varepsilon \text{eff\_fluid} = \left(\frac{3.54 * 10^9 * \left(\vartheta_{l(\text{rad})} - \vartheta_{s(\text{rad})}\right)}{f}\right)\text{^}2 \quad \text{Eq B.5}$$

$$\varepsilon r(\text{fluid}) = \frac{\varepsilon \text{eff\_fluid} - 3.2898}{0.3112} \quad \text{Eq B.6}$$

Case 2:-

Equations B.7 & B.8 use the frequency dependent board dielectric constant (Eq B.4) to find the relative permittivity of superstrate using equations B.1 & B.2. For the below equations the superstrate was the fluid.

$$\varepsilon \text{eff\_fluid} = \left(\frac{3.54 * 10^9 * \left(\vartheta_{l(\text{rad})} - \vartheta_{s(\text{rad})}\right)}{f}\right)^2 \quad \text{Eq B.7}$$

$$\varepsilon f(\text{fluid}) = \frac{\varepsilon \text{eff\_fluid} - 0.6875 * \varepsilon r(\text{board})}{0.3125} \quad \text{Eq B.8}$$

APPENDIX C

Complete Microstrip Test Setup Measurement and Procedure

C.1 Measurement Setup

Measurements are taken on the Anritsu 37369D Network Analyzer for the frequency 0.1 GHz to 14GHz. A full two-port calibration is done using the Anritsu Calibration SMA Kit. The number of points in the frequency range is chosen at 800. The equipment setup is shown in Fig C.1. The beaker containing the liquid has a thermometer to read the temperature of the fluid at any given point of time.

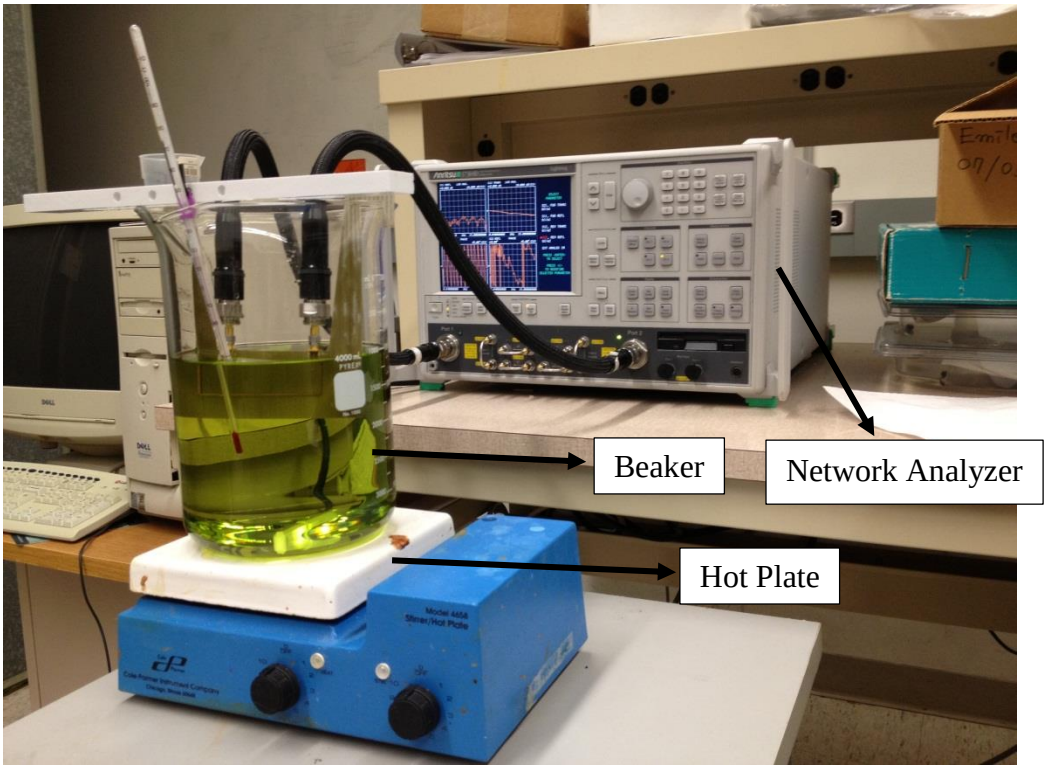

Figure C.1. Microstrip High frequency testing setup, with the microstrip line connected to the network analyzer and placed on a hot plate with a thermometer placed inside the beaker.

C.2 Measurement Procedure

The temperature of the fluid in the beaker is increased by turning the heat dial. The S parameter readings are recorded once the steady state desired temperature is read by the thermometer for a period of 10 minutes. The same procedure is repeated for subsequent temperature readings.

APPENDIX D

Dielectric Extraction Using Coplanar Waveguide

$$\varepsilon eff = (\frac{(\vartheta_{l(rad)} - \vartheta_{s(rad)}) * c}{2\pi f(l_l - l_s)})\text{^}2 \quad \text{Eq D.1}$$

For the extraction of the relative permittivity of the superstrate, two cases were considered:

1) Coplanar Waveguide without ground plane
2) Coplanar Waveguide with ground plane

Case 1:- The relationship between effective permittivity of the coplanar waveguide without back ground plane and the relative permittivity of the fluid is seen using equation D.2. Using Equation D.1 and D.4 the relative permittivity of the fluid/superstrate is extracted.

$$\varepsilon eff = \varepsilon f + \frac{\varepsilon r - \varepsilon f}{2} \frac{K(k2)}{K'(k2)} \frac{K'(k1)}{K(k1)} \quad \text{Eq D.2}$$

$$\varepsilon f = \frac{\varepsilon eff - \varepsilon f \frac{C}{2}}{1 - \frac{C}{2}} \quad \text{Eq D.3}$$

Where

$$C = \frac{K(k2)}{K'(k2)} \frac{K'(k1)}{K(k1)}$$

K( ) & K′( ) are the complete elliptical integrals of the first kind.

$$k_1 = \frac{a}{b} \sqrt{\frac{1-\frac{b^2}{c^2}}{1-\frac{a^2}{c^2}}} \quad , \quad k_2 = \frac{\sinh\left(\frac{\pi a}{2d}\right)}{\sinh\left(\frac{\pi b}{2d}\right)} \sqrt{\frac{1-\sinh 2\left(\frac{\pi b}{2d}\right)\sinh 2\left(\frac{\pi c}{2d}\right)}{1-\sinh 2\left(\frac{\pi a}{2d}\right)\sinh 2\left(\frac{\pi c}{2d}\right)}}$$

a = W/2, b=W/2+S, c=W/2+S+Wg

$$\varepsilon f(fluid) = \frac{\varepsilon eff - 1.963}{0.5894} \quad \text{Eq D.4}$$

Case 2:- The relationship between effective permittivity of the coplanar waveguide with back ground plane and the relative permittivity of the fluid is seen using equation D.5. Using Equation D.1 and D.7 the relative permittivity of the fluid/superstrate is extracted.

$$\varepsilon eff = \varepsilon f \frac{B}{A+B} + \varepsilon r \frac{B}{A+B} \qquad \text{Eq D.5}$$

$$\varepsilon f = \frac{\varepsilon eff - \varepsilon r \frac{B}{A+B}}{\frac{A}{A+B}} \qquad \text{Eq D.6}$$

where $A=K(k_3)/K'(k_3)$ & $B=K(k_4)/K'(k_4)$

$K( )$ & $K'( )$ are the complete elliptical integrals of the first kind.

$$k_3 = \frac{a}{b}\sqrt{\frac{1-\frac{b^2}{c^2}}{1-\frac{a^2}{c^2}}} \quad , \; k_2 = \frac{\tanh\left(\frac{\pi a}{2d}\right)}{\tanh\left(\frac{\pi b}{2d}\right)}$$

a = W/2, b=W/2+S, c=W/2+S+Wg

$$\varepsilon f(\text{fluid}) = \frac{\varepsilon eff - 2.7845}{0.41748} \qquad \text{Eq D.7}$$

APPENDIX E

PDMS FABRICATION AND CHANNEL OPERATION PROCESS

E.1 Glass Master Mold

Clear glass wafer mask of 2mm thickness is used to construct the Master mold.

a) The dicing saw is used to create 15x2, 15x4 and 45x45 mm^2, rectangular solid pieces of 2 mm thickness from the wafer mask.

b) The 15x2 and 15x4 mm^2 pieces act as channels, which are glued to the 45 mm glass substrate using an epoxy with 60 minutes cure time.

c) After the cure time the mold is cleaned with acetone/methanol/isopropyl alcohol.

d) The master mold is then placed in an aluminum foil boat for PDMS fabrication as seen in Fig E.1

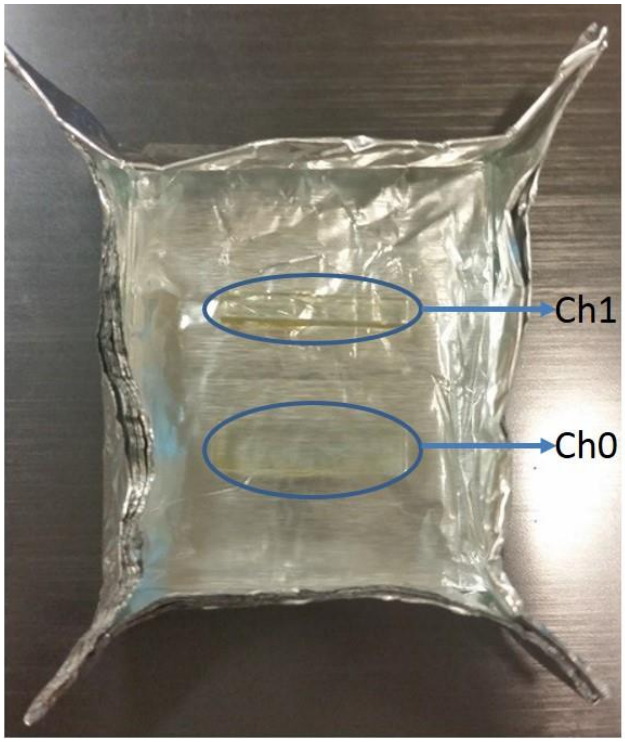

Figure E.1. Master mold in the aluminum foil boat

E.2 PDMS Fabrication

a) Pour PDMS (Dow Corning Sylgard 184) 10:1 (silicone: hardener) into the aluminum foil boat till the channels are covered.

b) This aluminum foil boat is then placed in the desiccation chamber for an hour to remove air bubbles in the mixture

c) Place the aluminum foil boat containing the master mold and the degassed PDMS in an oven at 120^0C for 3 hrs.

d) Remove the aluminum foil and slowly peel of the hardened PDMS from the glass master mold.

e) Inspect to ensure all the channels have been formed.

f) Cut desired PDMS dimensions by pushing straight down with razor blade.

g) Clean with acetone/methanol/isopropyl alcohol.

h) Use the PDMS adhesive (Dow Corning SE 9187L) at the edges of the PDMS to attach it to the FR4 board.

i) Make sure that the adhesive does not seep into the empty channels.

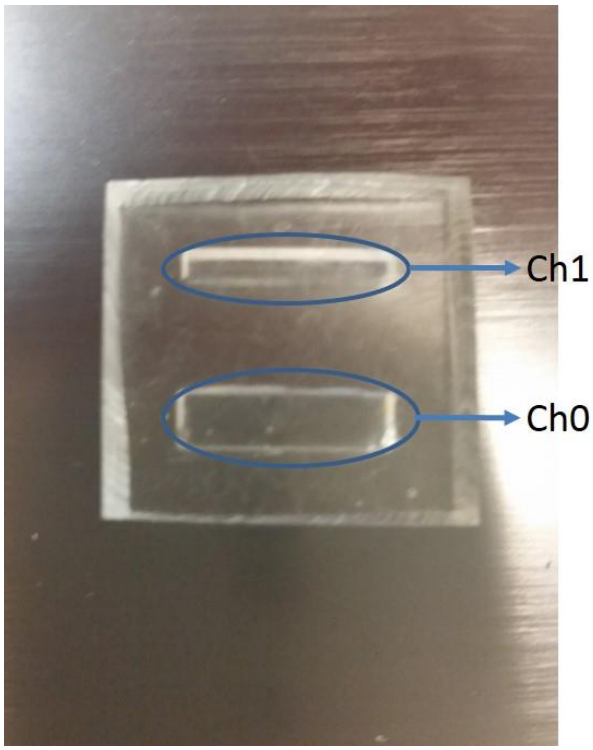

Figure E.2. PDMS housing with the channels

E.3 Fluid Operation Process

a) Use a 21 gauge syringe to punch a hole at the side of each channel.

b) This hole can be used to fill and remove the liquid with the use of a syringe.

c) Suck the air out of the channels with the syringe

d) While filling the channels with the liquid ensure that no air bubbles are introduced in this process. This can be done by pushing in the liquid very slowly.